The Structural Organization and Protein Composition of Lens Fiber Junctions

G. A. Zampighi,* J. E. Hall,‡ G. R. Ehring,‡ and S. A. Simon§

*Department of Anatomy, Jerry Lewis Neuromuscular Research Center, University of California at Los Angeles School of Medicine, Los Angeles, California 90024; ‡Department of Physiology and Biophysics, University of California at Irvine, Irvine, California 92717; and §Department of Neurobiology, Duke University Medical Center, Durham, North Carolina 27710

Abstract. The structural organization and protein composition of lens fiber junctions isolated from adult bovine and calf lenses were studied using combined electron microscopy, immunolocalization with monoclonal and polyclonal anti-MIP and anti-MP70 (two putative gap junction-forming proteins), and freeze-fracture and label-fracture methods.

The major intrinsic protein of lens plasma membranes (MIP) was localized in single membranes and in an extensive network of junctions having flat and undulating surface topologies. In wavy junctions, polyclonal and monoclonal anti-MIPs labeled only the cytoplasmic surface of the convex membrane of the junction. Label-fracture experiments demonstrated that the convex membrane contained MIP arranged in tetragonal arrays 6–7 nm in unit cell dimension. The apposing concave membrane of the junction displayed fracture faces without intramembrane particles or pits. Therefore, wavy junctions are asymmetric structures composed of MIP crystals abutted against particle-free membranes. In thin junctions, anti-MIP labeled the cytoplasmic surfaces of both apposing membranes with varying degrees of asymmetry. In thin junctions, MIP was found organized in both small clusters and single membranes. These small clusters also abut against particle-free apposing membranes, probably in a staggered or checkerboard pattern. Thus, the structure of thin and wavy junctions differed only in the extent of crystallization of MIP, a property that can explain why this protein can produce two different antibody-labeling patterns. A conclusion of this study is that wavy and thin junctions do not contain coaxially aligned channels, and, in these junctions, MIP is unlikely to form gap junction–like channels. We suggest MIP may behave as an intercellular adhesion protein which can also act as a volume-regulating channel to collapse the lens extracellular space.

Junctions constructed of MP70 have a wider overall thickness (18–20 nm) and are abundant in the cortical regions of the lens. A monoclonal antibody raised against this protein labeled these thicker junctions on the cytoplasmic surfaces of both apposing membranes. Thick junctions also contained isolated clusters of MIP inside the plaques of MP70. The role of thick junctions in lens physiology remains to be determined.

THE lens behaves functionally as a syncytium whose fluid balance is the integrated result of membrane transport properties of anterior epithelial and fiber cells, low resistance pathways connecting the fibers and epithelial cells, and restricted extracellular space between fibers (38, 39). Because the lens displays extensive networks of close plasma membrane appositions, it has often been argued that the low resistance pathways between fibers are the result of communicating "gap" junctions. Moreover, many of these junctional structures contain a 28-kD protein called MIP, which has been regarded as the gap junction–forming protein of the lens. Numerous studies have attempted to demonstrate that the lens junctions are gap junctions and that MIP belongs to the family of communicating proteins. These studies include morphological studies of junctions in the whole lens and in isolation (3, 9, 13, 18, 32–34, 36, 40, 45, 48, 49, 56, 64), biochemical characterization of the isolated fiber junctions (1, 2, 6, 7, 23, 24, 26, 28, 42, 43, 58), physiological studies of lens coupling (19, 38, 40, 51, 52, 55), immunolocalization of the major intrinsic membrane proteins (5, 13, 21, 29, 47, 54), and the determination of the amino acid sequence of MIP by cDNA methods (20, 53).

A reexamination of the criteria used for defining the presence of putative gap junctions containing MIP between lens fibers suggests that the situation may be more complicated than generally recognized (56, 64). Morphologically there are certainly a large number of closely apposed plasma membranes having the pentalamellar appearance associated with gap junctions. However, detailed morphological studies of isolated lens fiber plasma membranes have described different types of junctions (thick, thin, and wavy) based on overall thickness, surface topology, and arrangement of proteins in

the junctional plaques (56, 64). Also, these junctions occupy different regions in the lens. In the cortex the predominant junctions are thick and relatively straight, whereas in the nuclear regions junctions display an undulating surface topology and are thinner (9a).

MIP has been localized in lens fiber plasma membranes using immunocytochemical methods. Some studies reported that antibodies against MIP labeled thick junctions and some single membranes (5, 13, 54). Others reported antibody staining of single membranes only (47). Moreover, antibodies against MIP do not label gap junctions between the cells of the anterior lens epithelium (13) or between liver hepatocytes. Recent studies have shown that another protein, called MP70, is a major constituent of the thick junctions of the lens outer cortex (21, 29). In contrast to MIP, this junctional protein appears to be absent from wavy junctions in the nuclear regions and from single membranes. Therefore, immunocytochemical studies indicate that lens junctional membranes having slightly different structural organizations are constructed of different proteins.

The complete amino acid sequences of MIP, liver, heart, and *Xenopus* gap junction proteins have been deduced from cDNA cloning (4, 14, 20, 31, 46). Comparison of these sequences shows no homology between MIP and gap junction proteins from these tissues. Models based on sequence information suggest that liver and heart gap junction proteins have four transmembrane domains and that MIP has six. On the other hand, the sequence of the amino terminus of MP70 shows homology with the liver and heart proteins, suggesting that it may belong to the family of communicating proteins (30).

To clarify the structural organization of junctions containing MIP and MP70 and their roles in lens physiology, we undertook a detailed analysis of the structure and protein composition of the different types of isolated fiber junctions. We found that wavy junctions are constructed of tetragonal crystals of MIP in the convex membrane. These crystals abut the concave membrane which is particle free. In thin, flat junctions, MIP was arranged in both small clusters and single molecules. These small clusters also abut a particle-free apposing membrane, probably in a staggered or checkerboard pattern. Thus, wavy and thin junctions are not constructed of coaxial aligned channels, and, in these junctions, MIP is unlikely to form communicating channels. We suggest MIP may behave as an intercellular adhesion molecule that can also act as a volume-regulating channel. Its essential role could be to minimize the volume of the extracellular space.

Materials and Methods

Isolation

Frozen lenses from calf and adult bovines were obtained from Pel-Freeze Biologicals (Rogers, AR). Lenses were immersed in liquid nitrogen immediately upon collection and shipped in dry ice. Lens plasma membranes were isolated as described previously (64). The capsules of ~50 lenses were removed, and the lenses were cut into small pieces with a razor blade and homogenized in ~300 ml of solution A (2 mM $NaHCO_3$, 3 mM EDTA, and 100 μM PMSF adjusted to pH 8 with NaOH). In two experiments, the cortical and nuclear regions of calf lenses were processed separately. Plasma membrane fractions from cortical and nuclear regions were similar in their SDS-PAGE patterns and morphology and, therefore, the data will be presented without specifiying the region of the lens. After homogenization, the suspension was diluted to 1 liter with solution A and filtered twice through four layers of surgical gauze. The milky suspension was centrifuged at 2,000 *g* for 10 min (JA-14 rotor; Beckman Instruments, Inc., Fullerton, CA) and the large pellets were washed twice in the same solution. The pellets were resuspended in solution B (4 mM Tris base, 5 mM EDTA, 1 mM $CaCl_2$, 1.5 mM NaN_3, pH 8) and centrifuged at 2,000 *g* for 10 min. The pellets were extracted with 500 ml of 4 M urea in solution B and centrifuged at 17,000 *g* for 10 min (JA-17 rotor; Beckman Instruments, Inc.). The white portion of the pellets was then extracted with 150 ml of 7 M urea in solution B and centrifuged at 64,000 *g* for 90 min. The pellets were then resuspended in solution B and washed three times by centrifugation at 17,000 *g* for 10 min. After each centrifugation, the dark central region of the pellets was discarded. The isolated junctions were diluted with solution B (2–3 mg/ml), and 100-μl aliquots were stored at −80°C.

Electron Microscopy

Immunocytochemistry. Immunocytochemistry was performed by the method of Young et al. (62). Aliquots of lens junctional membranes (20 μl of a 2–3-mg/ml protein) were diluted to 200 μl with 3% BSA in PBS buffer for 30 min. The suspension was centrifuged 2 min in an Eppendorf table centrifuge (Brinkmann Instruments Co., Westbury, NY), and the pellets were resuspended in dilutions of the primary antibodies. The polyclonal anti-MIP (gift from Drs. D. Bok and J. Horwitz, Jules Stein Eye Center, UCLA) serum was diluted with filtered PBS buffer (0.2-μm pore size) at 1:100, 1:50, 1:10, and 1:5. The best results were obtained using the 1:10 dilution. With the monoclonals anti-MIP (gift from Drs. D. Paul and D. A. Goodenough, Department of Anatomy and Cell Biology, Harvard Medical School) and anti-MP70 (gift from Dr. J. Kistler, Department of Cell Biology, Auckland, New Zealand), the supernatant fluids from the cell cultures were used undiluted.

Isolated junctions (20 μl of a 2–3-mg/ml protein) suspended in the primary antibodies (100–200 μl) were incubated for 2 h at room temperature. After incubation, the junctions were washed three times in 200 μl of PBS buffer filtered by centrifugation in an Eppendorf table centrifuge (Brinkmann Instruments Co.) for 2 min. The pellets were resuspended in 100 μl of solution containing secondary antibodies. The polyclonal anti-MIP was visualized with protein A–gold particles with diameters of 5 and 15 nm (E. Y. Laboratories, Inc., Biochemical Division, San Mateo, CA). Protein A–gold solutions provided by the manufacturer were diluted 1:1 with PBS buffer. The monoclonals were visualized with an antibody to mouse IgM, complexed with peroxidase (Chemicon Inter. Inc., El Segundo, CA) at a dilution of 1:100 with PBS buffer. The anti-MP70 monoclonal was also visualized with anti–mouse IgM conjugated with 10-nm-diam gold particles (Sigma Chemical Co., St. Louis, MO). In all cases the samples were incubated at room temperature for 2 h.

Double labeling using the polyclonal anti-MIP, visualized with protein A–gold (5- and 15-nm particle diameter), and monoclonal anti-MP70 visualized with anti–mouse IgM conjugated to 10-nm-diam gold particles was also performed in isolated junctions. The procedure was the same as the one described for single labeling except that the two antibodies were used sequentially. In some experiments anti-MIP was used first while in others anti-MP70 was used first. Protein A–gold was always used before the anti–mouse IgM conjugated with gold particles because of the slight cross reaction between the two probes.

The peroxidase reaction was carried out with 0.1% diaminobenzidine using hydrogen peroxide as a substrate. Junctions were washed three times by centrifugation with PBS buffer and the resulting pellets were then processed for thin sectioning and label-fracture electron microscopy.

Thin Sectioning. Aliquots of the isolated membranes (20 μl of a 2–3-mg/ml protein) were diluted to 200 μl with 0.2 M Na cacodylate buffer, pH 7.3, and then spun down in an Eppendorf table centrifuge (Brinkmann Instruments Co.) for 2 min. The membranes were fixed as pellets in 2–3% glutaraldehyde in 0.2 M Na cacodylate buffer for 1 h at room temperature whereupon the fixative solution was changed to 2–3% glutaraldehyde with 0.5% tannic acid for 30 min. The pellets were then washed extensively with several changes of 0.2 M Na cacodylate for 1 h and postfixed in 2% osmium tetroxide in 0.1 M Na cacodylate for 90 min at room temperature. The pellets were washed (three changes) with 0.2 M Na acetate, pH 5, and block stained in 0.1 M Na acetate with 0.25% uranyl acetate overnight. The pellets were dehydrated in ethanol, passed through propylene oxide, and embedded in Epon 812 as described previously (53, 54). Sections (silver-to-gray interference color) were cut in an ultramicrotome (MT5000; Sorvall Instruments Div., Newton, CT) with a diamond knife. The sections were placed on top of formvar-coated single-hole grids and stained with aqueous solutions of uranyl acetate and lead.

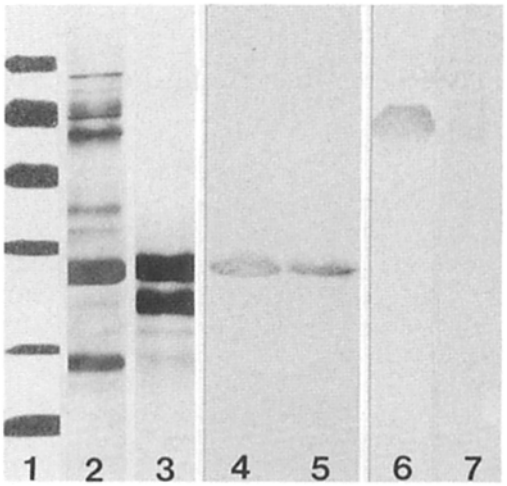

Figure 1. Comparison by SDS-PAGE of membranes isolated from calf lenses (lane *2*) and from adult bovine lenses (lane *3*) to demonstrate the decrease in the number of protein bands with aging. Also, membranes isolated from adult bovine lenses contained higher concentrations of MP22, an endogenous proteolytic fragment of MIP (lane *3*). Standards are shown in lane *1*: phosphorylase b, 94,000; BSA, 67,000; ovalbumin, 43,000; carbonic anhydrase, 30,000; soybean trypsin inhibitor, 20,100; alpha-lactalbumin, 14,400. Loading was ~12 μg of protein per lane and the gels were stained with Coomassie blue. Western blots of junctional fractions isolated from calf (lane *4*) and adult bovine (lane *5*) lenses were labeled with the monoclonal anti-MIP. Note that both fractions contained MIP at high concentrations. In contrast, Western blots of these fractions with the monoclonal anti-MP70 showed high concentrations of MP70 only in membranes isolated from calf lenses (lanes *6* and *7*). MP22 was not labeled by the monoclonal anti-MIP (lanes *4* and *5*).

Freeze-Fracture. Freeze-fracture experiments were performed by adhering the isolated unfixed and unglycerinated junctions to a positively charged glass surface (8, 9, 11). Glass coverslips were washed with a concentrated solution of 7× Linbo detergent, polished with a dispersion of detergent and alumina powder, and washed extensively in distilled water. Positive charges were absorbed on the clean glass surface by immersing the glass in a solution containing 0.1% Alcian blue. The coverslips were air dried and cut with a diamond pencil into strips that fit the Freeze-Fracture-Etch cold stage (Balzers S. p. A., Milan). The junctions (0.1–0.5 μl) were spread upon the charged glass surface and thinned by removing excess solution with filter paper. The thin film of membranes adhering to the glass surface was covered with a copper hat (Balzers S. p. A.) previously etched with concentrated nitric acid. The membranes sandwiched between the copper hat and the glass surface were then frozen by immersion in liquid propane. The sandwiches were then transferred under liquid nitrogen to a freeze-fracture apparatus (400K; Balzers S. p. A.) and fractured at −150°C and at a vacuum of 10^{-7} mbar by removing the copper hat with one pass of the cold knife. The glass surface containing the fractured junctions was shadowed with Pt-C at 45°C and carbon at 90°C. The membranes were digested for 30 min in 5.25% Na hypochlorite (Purex bleach), and the replicas were washed by transferring them to three successive distilled water baths for ~10 min each. The replicas were placed on single-hole grids covered with formar, as described previously (66).

Label-Fracture. For label-fracture experiments, unfixed, unglycerinated aliquots of junctions labeled with anti-MIP and visualized with protein A–gold were adhered on positively charged glass surfaces and covered with copper hats. The sandwiched junctions were processed as described for freeze-fracture (see above). The replicas were washed in distilled water (not in bleach) and collected on formar-coated single-hole grids.

This variation of the label-fracture technique of Pinto da Silva and Khan (50) was found to be technically simple, very reproducible, and able to produce clean replicas. More importantly, the replicas contained extensive membrane fracture faces labeled with gold particles. The fracture faces were flat (since the membranes were adhered to glass) and thus the interpretation of the fracture planes was straightforward because the glass surface served as the reference plane.

Other Methods

Protein concentration was determined by the method of Lowry et al. (37). The specificity of the antibodies against MIP and MP70 were determined by transferring the antigens from 12% SDS-PAGE into pure nitrocellulose membranes (Trans-blot; Bio-Rad Laboratories, Richmond, CA). The transfer was performed in an electrophoresis unit (Transphor; Hoefer Scientific Instruments, San Francisco, CA) at 0.6–0.8 A for 45 min. The membranes were incubated with the different antibodies and visualized with secondary antibodies complexed with peroxidase.

Results

Western Blots

SDS-PAGE analyses of plasma membranes isolated from calf lenses exhibited at least 14 protein bands (Fig. 1, lane *2*) while membranes isolated from adult bovine lenses (lane *3*) contained almost exclusively MIP and an endogenous proteolytic fragment of MIP called MP22 (24, 42). Immunoblots using the monoclonal anti-MIP show that MIP was present in plasma membranes isolated from both calf and adult bovine lenses and that MP22 was not recognized by this antibody (lanes *4* and *5*). On the other hand, immunoblots using the monoclonal anti-MP70 showed that this antibody recognized a protein band having an apparent molecular mass of 70 kD (29). MP70 is abundant in plasma membranes isolated from calf lenses (lane *6*), but not in plasma membranes isolated from lenses of adult animals (lane *7*).

Thin Sectioning

Fractions isolated from calf lenses contained extensive, flat thin and thick junctions, small round (0.2–0.4-μm-diam) membrane profiles, and wavy junctions (Fig. 2 *A*, *arrows*). Thin and thick junctions appeared as large circular profiles that could not be distinguished from each other at low magnifications (Fig. 2 *A*). Wavy junctions were easily identified by their undulating surface topology with a wavelength of 0.15–0.3 μm (Fig. 2 *A*, *arrows*). On the other hand, fractions isolated from lenses of adult animals contained almost entirely wavy junctions (Fig. 2 *B*). These junctions appeared, at higher magnifications, as pentalamellar structures comprised of two closely apposed plasma membranes (Fig. 2 *C*).

In plasma membranes isolated from calf lenses, thin, thick, and wavy junctions coexisted in the same junctional profiles separated by abrupt transitions (Fig. 3, *A* and *C*). Thin and thick junctions differed in the width of the layer of stain in the cytoplasmic surfaces (Fig. 2) and also in the distance between the centers of their hydrophobic cores. This distance measured 5.7 nm for thin and wavy junctions and 7.2 nm for thick junctions (Table I). This measurement includes the width of two half-membranes and the entire width of the extracellular gap. Fig. 3 *C* displays a junctional profile containing thin, wavy, and thick junctions separated by abrupt transitions. Thin and thick junctions differed in the width of the layer of stain on the cytoplasmic surfaces (Fig. 3, *A* and *B*). The wavy junction was identified by its pronounced curvature and also by its convex membrane appearing thicker than the concave one (Fig. 3 *C*). The small cross-sectional width of the concave membrane could be explained by a different lipid composition of the two apposing membranes or

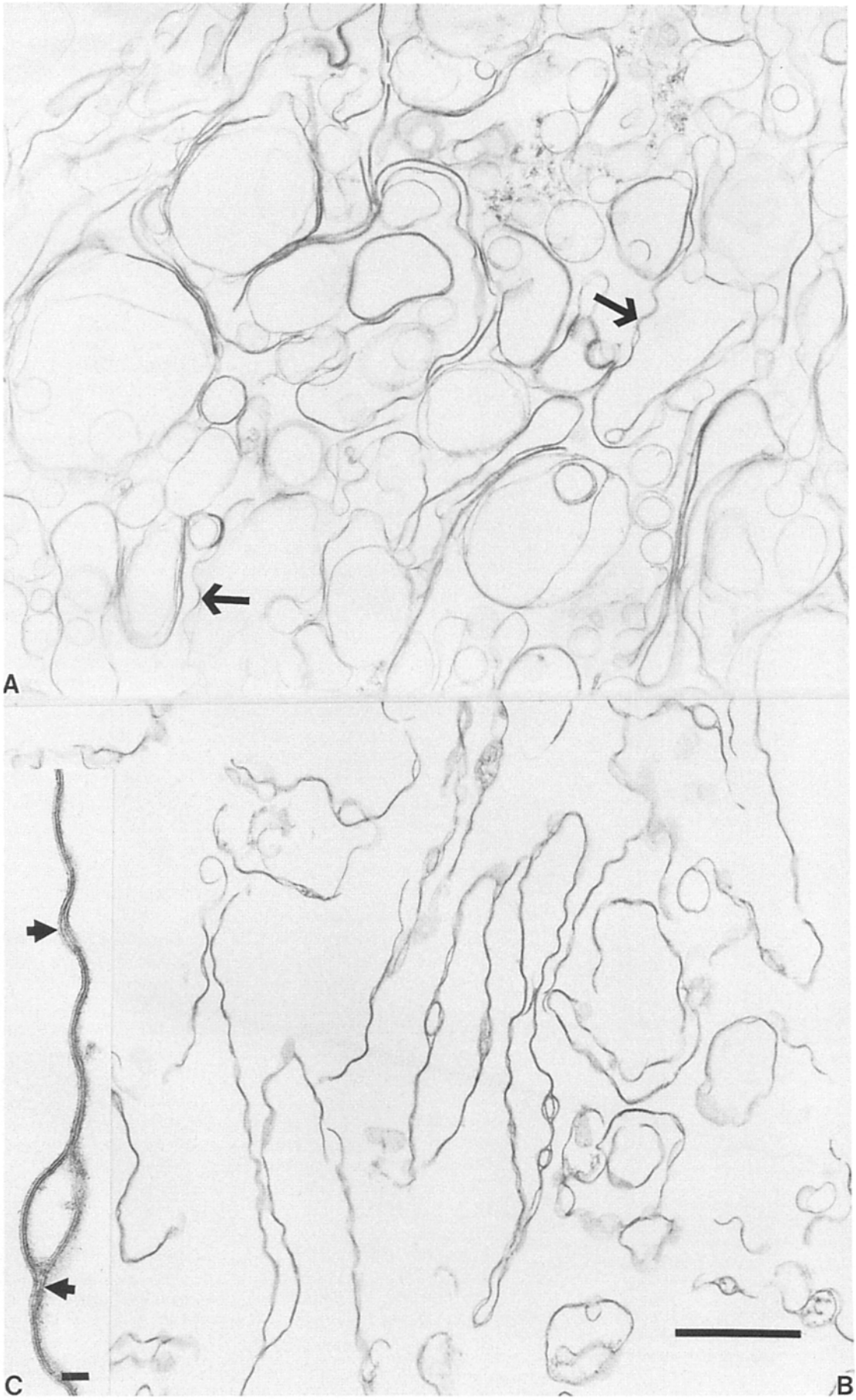
A
C
B

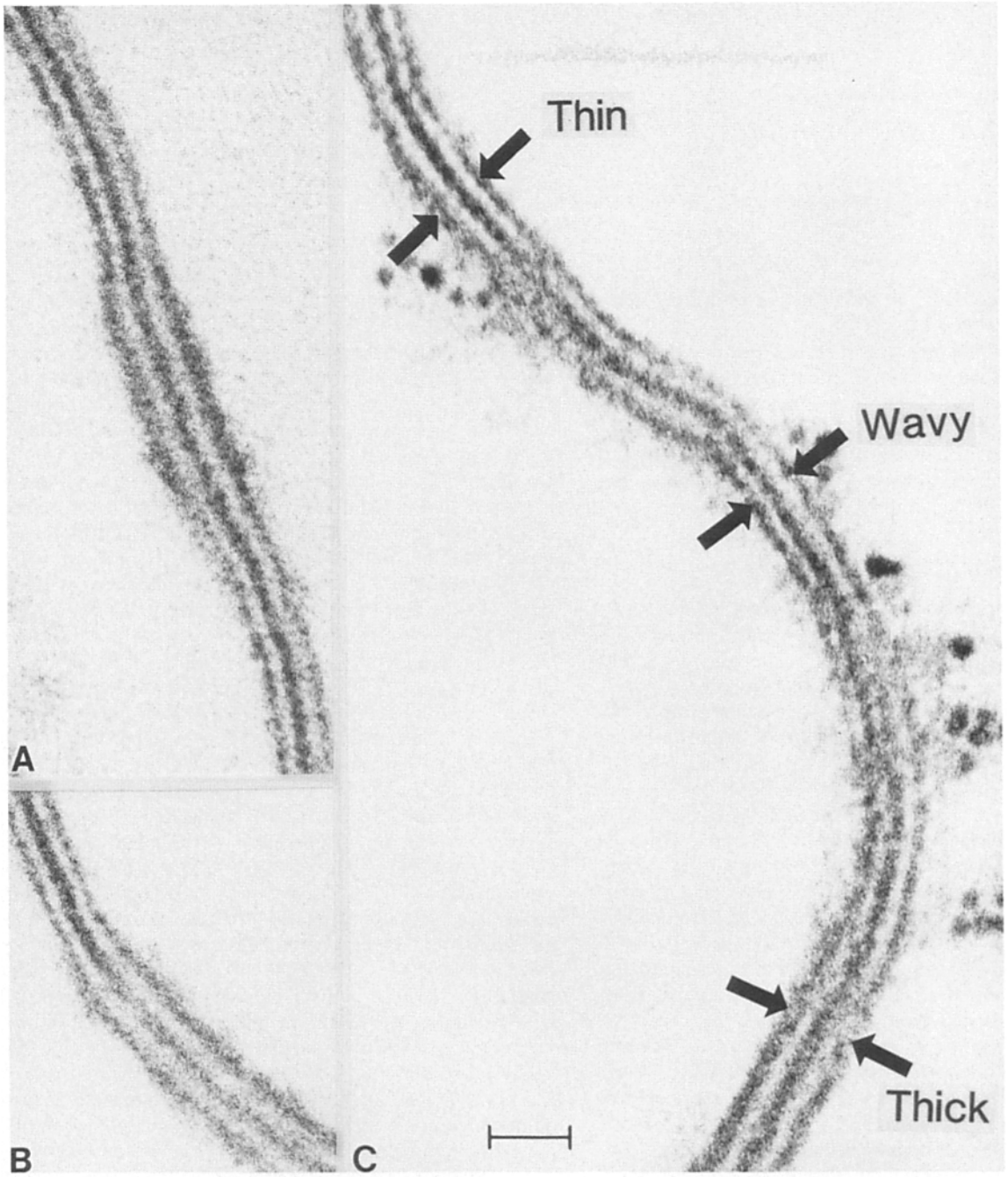

Figure 3. Higher magnification views of three types of lens junctions—wavy, thin, and thick—coexisting in the same profile. *A* and *B* show that abrupt transitions separate thin and thick junctions. The different junctional types were easily distinguished by the width of the dense layer on the cytoplasmic surfaces. Thick junctions were characterized by an overall thickness of 18–20 nm and the presence of thicker layers of stain at their cytoplasmic surfaces. Thin junctions were characterized by thinner bands of stain at the cytoplasmic surfaces and an overall thickness of 11–13 nm. *C* shows that the three types of junctions separated by abrupt transitions coexisting in the same profile. The concave membrane of wavy junctions appeared substantially thinner than the convex membrane. Bar, 20 nm.

Figure 2. A and *B* compare the appearance of membrane fractions isolated from lenses of calf and adult animals, respectively. Fractions isolated from calf lenses contained large round profiles that corresponded to thin and thick junctions and undulating profiles of the wavy junctions (*A*, *arrows*). The fractions isolated from adult bovine lenses contained primarily wavy junctions (*B*). Wavy junctions displayed a pentalamellar structure (three dense bands separated by two light bands) of 11–13 nm in overall thickness (*C*). The arrows in *C* point to regions where the two apposing membranes were separated by large spaces. Wavy junctions isolated from adult bovine lenses also contained biconvex vesicles displaying pentalamellar structures (*B* and *C*). Bars: (*A* and *B*) 1 μm; (*C*) 20 nm.

Table I. Structural Characteristics of Lens Junctions

Topology	Wavy	Thin	Thick
Overall thickness (nm)	11–13	11–13	18–20
Distance between hydrophobic cores*	5.7 ± 0.27 (21)	5.7 ± 0.33 (12)	7.2 ± 0.32 (26)
Stain pattern for MIP	Asymmetric	Symmetric	Small domes
Stain pattern for MP70	None	None	Symmetric
Width extracellular gap‡	0.7	0.7	2.2

* The measurements are mean ± SD. The numbers in parentheses indicate the number of measurements.
‡ Assuming a membrane thickness of 5 nm (35).

as an artifact produced by a curved surface projecting in the transverse plane (64).

Therefore, although all three types of lens junctions displayed pentalamellar structures consisting of two plasma membranes apposed through their external surfaces, they differed in their surface topology, their overall thickness, and the width of the extracellular gap (Table I). We will now present evidence that these different junctional structures have different protein compositions.

Labeling with Anti-MIP and Anti-MP70

Wavy junctions isolated from calf and adult bovine lenses displayed a distinctive alternating pattern when labeled with polyclonal and monoclonal anti-MIPs. The labeling pattern was closely related to the periodicity of the wave. Specifically, antibody molecules were visualized on the cytoplasmic surface of the convex membrane (the peak of the wave) but were absent from the apposing concave membrane (Fig. 4). Such specific localization of MIP in wavy junctions was also ascertained by direct visualization of antibody molecules on the cytoplasmic surface of the convex membranes. The antibody molecules appeared as an electron-lucent band located between the cytoplasmic surface and the layer of gold particles (Fig. 4 *D*). Because wavy junctions isolated from lenses of adult animals displayed very regular undulations (Fig. 2 *B*), their staining with anti-MIPs showed the alternating pattern (convex membranes labeled, concave membranes unlabeled) over extensive regions (data not shown).

The specific labeling of the convex membrane of wavy junctions observed with the polyclonal anti-MIP (Fig. 4) was confirmed by repeating the experiment using a monoclonal anti-MIP. The black arrows in Fig. 5 point to wavy junctions labeled on the convex membranes but not the apposing concave membranes. The polyclonal and monoclonal anti-MIPs also labeled the cytoplasmic surface of single membranes included in the extensive junctional profiles (Fig. 4 *A*, *black arrows*) and the round (0.2–0.4-μm-diam) vesicles. The polyclonal and monoclonal anti-MIPs did not label thick junctions (Fig. 4, *C* and *D*), an observation in good agreement with the studies of Paul and Goodenough (47). The lack of labeling on thick junctions was validated directly in images where both types of junctions appeared close to each other (Fig. 4 *C*) and in profiles where thick and wavy junctions were continuous with each other. In these profiles, gold particles were observed exclusively on wavy junctions (Fig. 4 *D*). Therefore, the absence of labeling of thick junctions is not a problem of antibody penetration but a demonstration that these junctions lack epitopes which the MIP antisera can recognize. Thus, both monoclonal and polyclonal anti-MIPs demonstrated that this protein is located in the convex membrane of wavy junctions only (Figs. 4 and 5). The same labeling pattern is observed with two different antibodies against the same protein; this represents a more direct and positive control than incubating these junctions with preimmune serum.

Immunolocalization of MIP on the cytoplasmic surfaces of both apposing junctional membranes had been reported in previous studies (5, 54). In wavy junctions isolated from adult animals, we have also observed labeling on cytoplasmic surfaces of both apposing membranes only on short junctional segments located at regions where the curvature of the wave reversed (Fig. 4 *B*). In fractions isolated from lenses of calves, on the other hand, the antibodies labeled extensive, flat, and thin junctions on both apposed membranes (Fig. 5, *black arrows*). These extensive junctional membranes were similar to the junctions stained with anti-MIP complexed with ferritin molecules (5) or gold particles (54). However, when the anti-MIP was visualized with peroxidase (Fig. 5), we observed that the labeling on both cytoplasmic surfaces was not completely symmetrical. The layer of stain located on one membrane was usually thicker than the layer on the apposing (Fig. 5, *open arrows*, and Fig. 5 *A*, *arrowheads*). This asymmetry in the staining was not observed clearly when the antibodies were visualized with gold particles, probably because the peroxidase reaction greatly amplified the signal. The asymmetry in the labeling of the junctional membranes is important because it points to the presence of

Figure 4. Junctions isolated from calf lenses labeled with the polyclonal anti-MIP and visualized with protein A–gold (15-nm particle diam). *A* shows an extensive, heavily stained junction combining wavy and thick components. The two black arrows indicate regions of single membranes labeled by the antibody. Note that gold particles were located on the convex membrane of wavy junctions but absent on the apposing membrane. The extensive, unlabeled region pointed to by the open arrow corresponds to a thick junction. *B–D* show higher magnification views of wavy and thick junctions. These views demonstrate specific labeling on the cytoplasmic surface of wavy junctions, the lack of staining of thick junctions, and the labeling of single membranes. When the curvature of the wave reverses, the location of the gold particles also reverses to became associated with the convex membrane of the opposing membrane (*B*, *arrows*). At these regions where the curvature reverses, short junctional segment display gold particles on both junctional membranes. *D* is a higher magnification of a region in *C* showing an unlabeled thick junction located between two asymmetrically labeled wavy junctions (*D*, *open arrow*). Bars: (*A*) 0.32 μm; (*B* and *C*) 0.1 μm; (*D*) 50 nm.

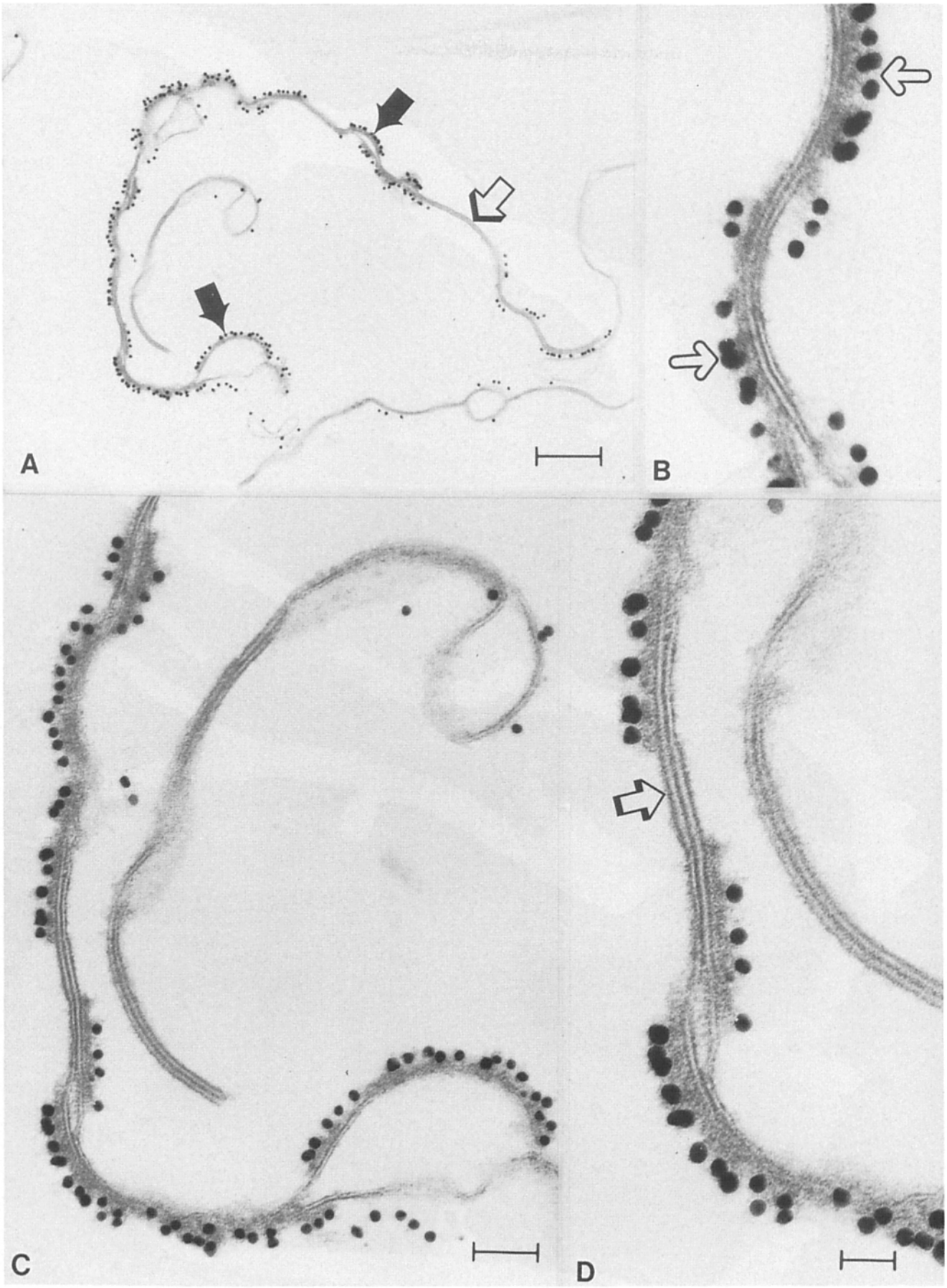
A
B
C
D

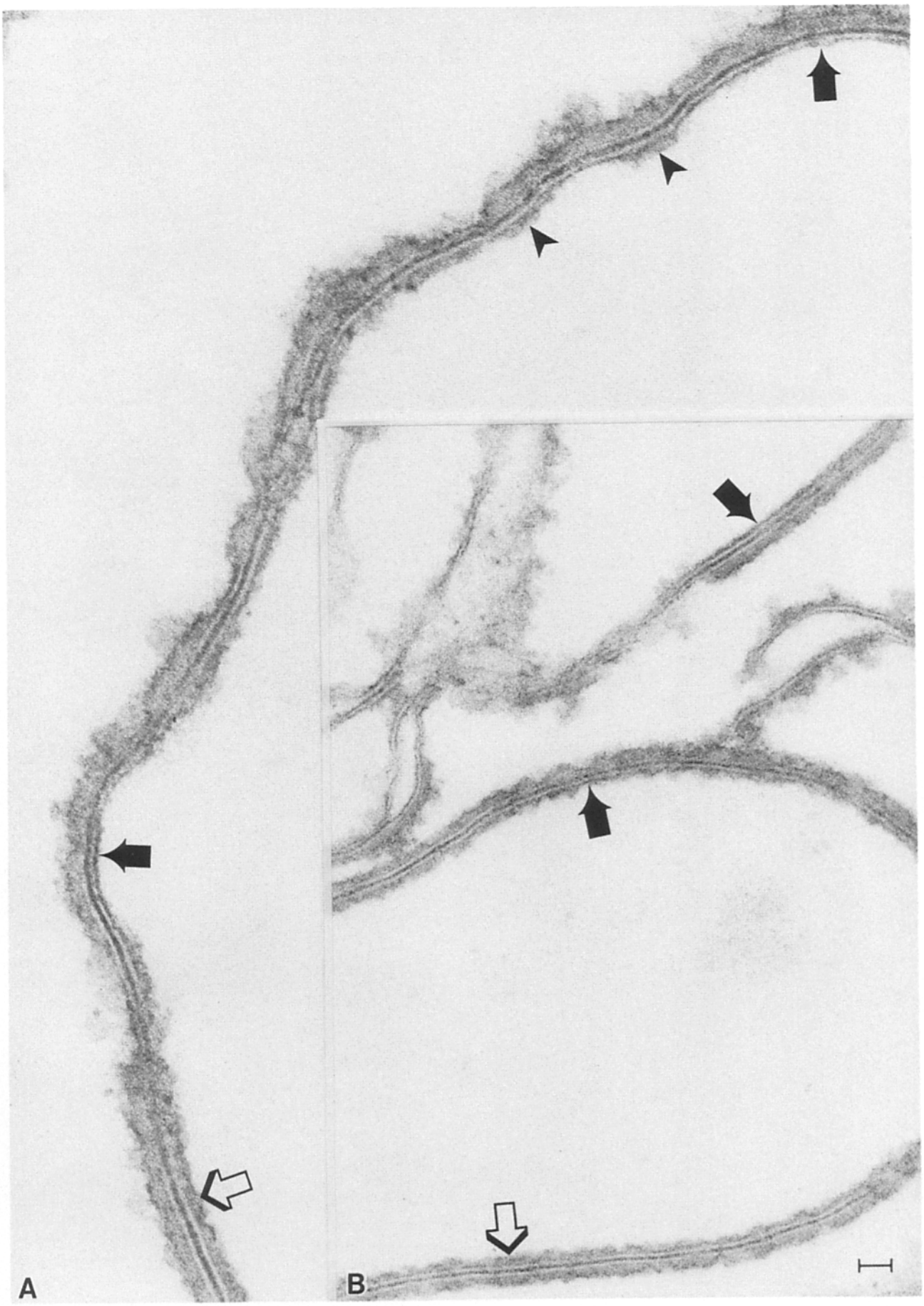
A
B

an unequal distribution of MIP molecules on the apposing membranes of thin junctions, which, as shown later, was also observed in label-fracture experiments.

Thus, monoclonal and polyclonal antibodies localized MIP in single membranes, with varying degrees of asymmetry in both apposing membranes of thin junctions, but exclusively in the convex membrane of wavy junctions. The fact that the frequency of thin junctions is greatly increased in calf lenses may reconcile conflicting immunolocalizations of this protein in previous studies (5, 13, 29, 47). Models attempting to explain the physiological role of MIP in lens fibers must take into account the presence of the protein in all these membranes.

Anti-MP70 labeled extensive thick junctions on both cytoplasmic surfaces (Figs. 6 and 7). In experiments where anti-MP70 was visualized with peroxidase, the pentalamellar structures were identified as thick junctions by measuring the distance between the centers of the hydrophobic cores (Table I). In experiments where anti-MP70 was visualized with gold particles, the junctional profiles were identfied as thick junctions by measuring their overall thickness and the distance between the hydrophobic core centers. As described previously (21, 29), anti-MP70 did not stain wavy junctions or single membranes (Figs. 6 and 7). The lack of staining of thin junctions and single membranes was determined in profiles where both types of membranes were continuous with each other. In these profiles, the labeled thick junctions were separated from the unlabeled thin and wavy junctions by abrupt transitions (Fig. 7, *C–E*, *black arrows*).

Double Labeling

To support the observation that thin and wavy junctions were composed of MIP and thick junctions of MP70, we performed experiments where the same fraction was labeled sequentially with anti-MIP and anti-MP70. The most convincing results from this experiment come from junctional profiles containing thin, wavy, and thick junctions. Fig. 8 shows one of these profiles composed of thick and wavy junctions from a fraction double labeled with anti-MIP and anti-MP70. Anti-MP70 (larger diameter gold particles) labeled both cytoplasmic surfaces of thick junctions. The junctions were identified by their overall thickness and the distance between the centers of their hydrophobic cores. Anti-MIP (small diameter gold particles) labeled only one junctional membrane as would be expected for wavy junctions (Fig. 8, *arrows*). The segregation of the probes depended exclusively on the structure of the junctions and was independent of the sequence of labeling and diameter of the gold particle used to visualize the antibodies (data not shown).

Freeze-Fracture

The two-dimensional organization of protein units in lens fiber junctions was determined by freeze-fracture electron microscopy. At low magnification, wavy and thick junctions were recognized by their surface topologies (Fig. 9). Detailed analysis of the fracture faces demonstrated that both types of junctions fractured conventionally, leaving particles on the PF and complementary pits on the EF fracture faces. The fact that the fracture faces corresponded to junctions instead of single membranes was ascertained by measuring the height of the fracture step separating the EF from the PF faces (Table I). Since junctions are comprised of two membranes joined at their external surfaces, the height of the fracture step separating EF and PF faces is equivalent to the distance between the centers of their hydrophobic cores measured in transverse thin sections. After correcting for the shadowing angle, the height of the fracture step was calculated to be 7 $\pm$ 0.3 nm (mean $\pm$ SD, n = 14) for thick junctions and 5.5 $\pm$ 0.7 nm (mean $\pm$ SD, n = 22) for thin junctions. The measurements were obtained from unfixed, unglycerinated junctions and, thus, are not affected by shrinkage resulting from fixation and dehydration.

The flat and undulating surface topologies of thin, thick, and wavy junctions represented two extremes of organization whose relative frequency of appearance depended on lens fiber age. Fractions isolated from calf lenses, on the other hand, displayed flat and wavy junctions in the same fracture faces (Fig. 10). The fracture faces of the thin junctions contained particles on the PF and pits on the EF, while the wavy junctions appeared as dome-shaped regions of 0.3–0.4 μm in diameter (Fig. 10, *B–E*). The center of the domes contained tetragonal arrays of 6–7 nm in unit cell dimension (Fig. 10, *B–E*). Surrounding these arrays, bands of smooth fracture faces ~65 nm wide, separated the crystalline patches from the faces of flat junctions having particles and pits arranged without crystalline order. When the fracture plane passed across the domes, the height of the fracture step separating EF from PF faces revealed that the width of the extracellular space at the domes was greatly increased (Fig. 10, *D* and *E*). Therefore, the domes correspond to single membranes, and the tetragonal arrays of particles and pits do not form coaxially aligned gap junction–like channels. The domes seen in Fig. 11, *D* and *E*, most likely correspond to the curved single membranes labeled with the anti-MIP in thin sections (Fig. 4 *A*, *black arrows*). Previous studies have reported extensive tetragonal arrays in the EF and PF fracture faces separated by fracture steps of small height (3, 48, 49). However, the fracture steps separating EF from PF faces were not located inside the crystalline patches but at the boundaries between adjacent patches. Thus, these images do not demonstrate that apposing tetramers form coaxially aligned channels.

Label-Fracture

The localization of MIP in lens fiber junctions was also de-

Figure 5. The specific labeling of the convex membrane of the wavy junction, seen with the polyclonal anti-MIP (Fig. 4), was also observed when junctions were labeled with a monoclonal anti-MIP visualized with peroxidase. The black arrows point to wavy junctions labeled exclusively at the convex side, an observation that confirms the asymmetric staining pattern described with the polyclonal anti-MIP. The open arrows point to junctions stained at both cytoplasmic sides with varying degrees of asymmetry. Although the staining in these flat junctions appeared on both junctional membranes, usually one membrane contained a thicker layer of stain than the opposing membrane (*A*, *arrowheads* and *open arrows*). A possible explanation of this staining pattern is that the two junctional membranes contain unequal distributions of MIP molecules. Bar, 21.4 nm.

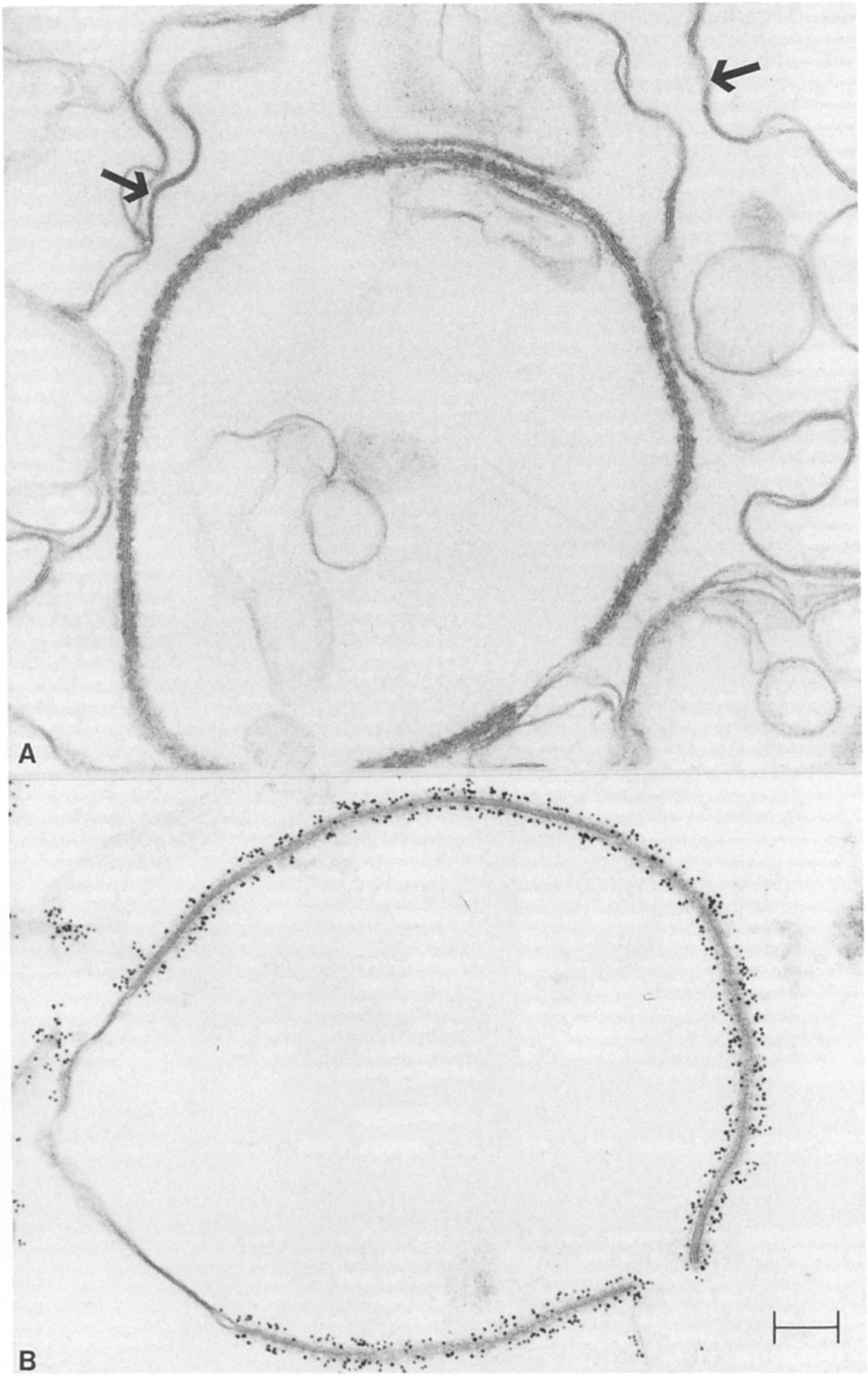
A
B

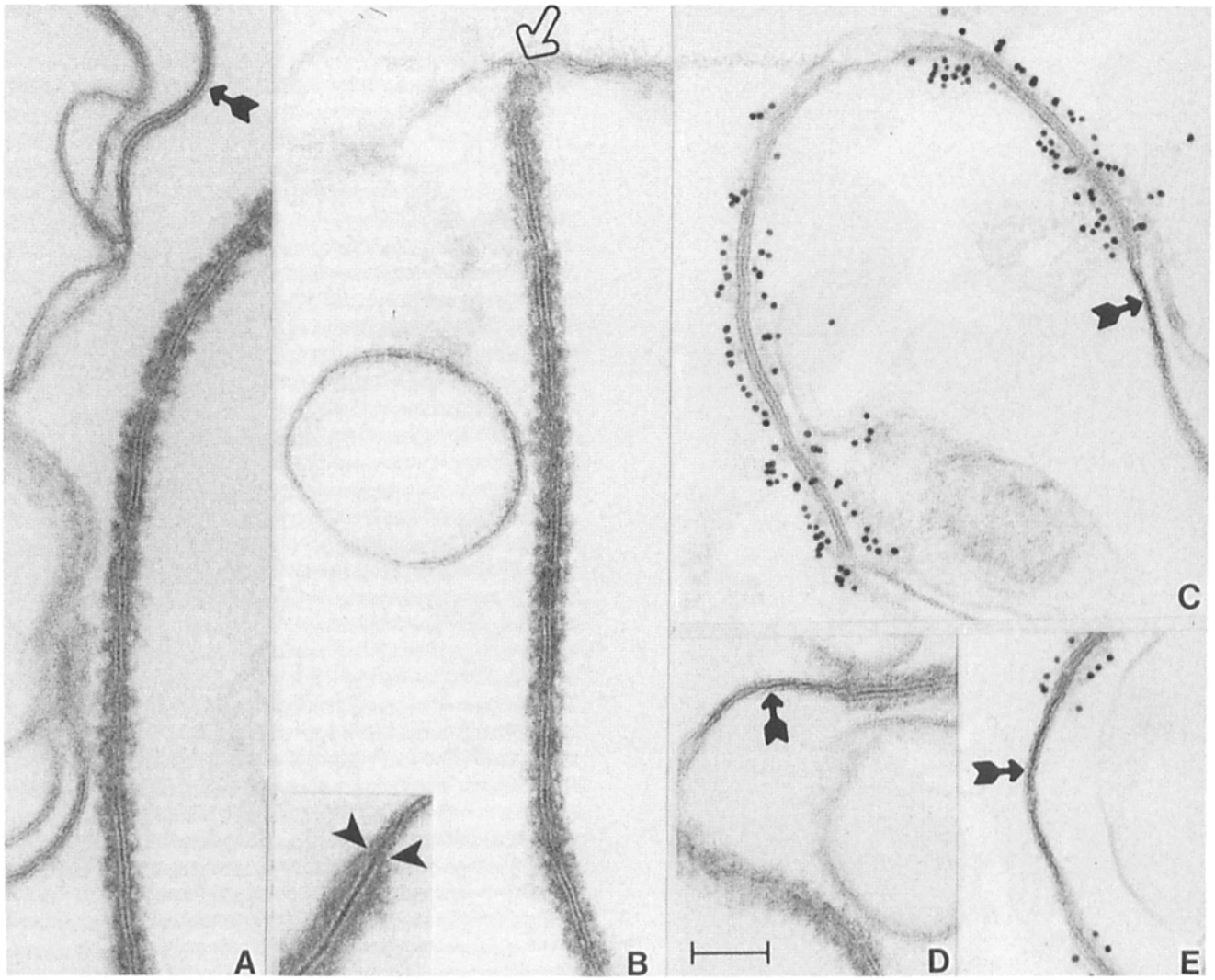

Figure 7. Higher magnification views of thick junctions labeled with anti-MP70 and visualized with gold particles (*C* and *E*) and peroxidase (*A*, *B*, and *D*). Both cytoplasmic surfaces were labeled when the antibody was visualized with either gold particles or peroxidase. Wavy and thin junctions, round membrane profiles (*B*), and single membranes (*B*, *open arrow*) were not labeled. The abrupt transitions between labeled thick junctions and unlabeled thin junctions are shown in *D* and *E*. Bar, 0.1 μm.

termined using a modification of the label-fracture technique developed by Pinto da Silva and Khan (50). This technique permits identification of the type of protein(s) composing individual intramembrane particles on the fracture faces of the membranes. The variation introduced in this paper is technically simple, very reproducible, and able to produce extensive fracture faces labeled with gold particles. The interpretation of the fracture faces was straightforward because the glass surface provides a definitive reference plane. Since junctions can only adhere to the glass via their cytoplasmic surfaces, all PF faces came from the membrane that adhered to the glass and all EF faces from the apposing junctional membrane. Junctions were distinguished from single membranes because their EF and PF faces were separated by fracture steps of small height. Figs. 11 and 14 show fracture faces from junctions labeled with the polyclonal anti-MIP visualized with gold particles. Unlike intramembrane particles that are exposed on the fracture surfaces, the gold particles do not cast shadows and consequently must be located between the supporting glass surface and the fractured membranes (Fig. 12). Gold particles were absent from the fracture faces of thick junctions (Figs. 13 and 14, *open triangles*), from exten-

Figure 6. Fractions isolated from calf lenses and labeled with the monoclonal anti-MP70 were visualized with peroxidase (*A*) and gold particles (*B*). The monoclonal anti-MP70 labeled exclusively thick junctions. The numerous wavy junctions (*A*, *arrows*) and single membranes vesicles were unstained with either visualization procedure. In profiles where thick junctions coexisted with segments of thin junctions and single membranes, the staining remained associated exclusively with thick junctions. Bar, 0.16 μm.

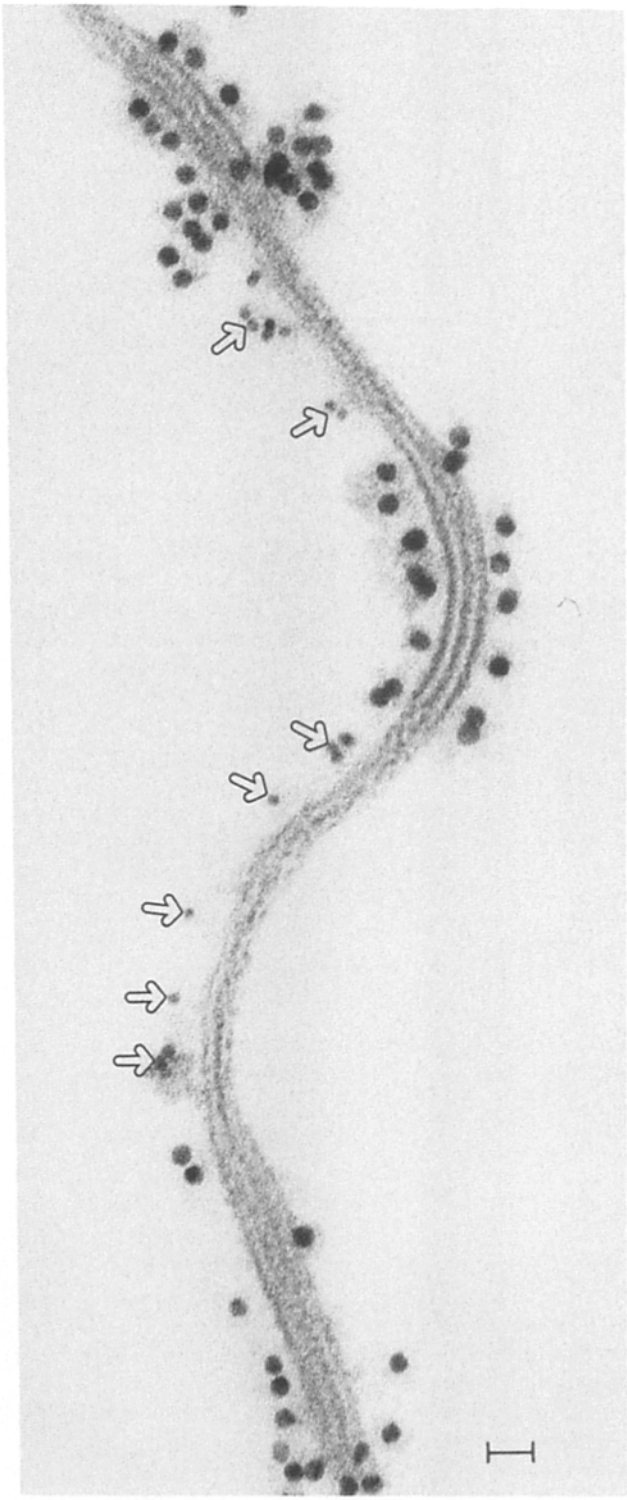

Figure 8. Double labeling of junctions isolated from calf lenses with the polyclonal anti-MIP visualized with 5-nm-diam gold particles (*arrows*) and the monoclonal anti-MP70 visualized with 10-nm-diam gold particles. The junctional profile contains three thick junctions separated by two wavy junctions. Thick junctions were labeled on the cytoplasmic surfaces of both membranes with the anti-MP70 while wavy junctions were stained only on one membrane with the anti-MIP (*arrows*). Therefore, the differences in surface topology and overall thickness between the different type of lens junctions are associated with different protein composition. Bar, 21.4 nm.

sive, smooth PF faces (Fig. 13, *PF*), and from the glass surface (Fig. 14).

The fracture faces of thick junctions were identified from the height of the fracture step separating EF from PF fracture faces and from the presence of particles and pits organized without crystalline order. Fracture faces from thick junctions contained few gold particles and, therefore, small amounts of MIP (Fig. 11). When gold particles were present in thick junctions, they were confined to small clusters distributed throughout the junctional plane. Frequently, these clusters were separated from the fracture faces of thick junctions by regions of membrane having smooth PF and EF faces. The fracture faces of thin and wavy junctions, on the other hand, displayed a large number of gold particles, indicating that they contained higher concentrations of MIP (Figs. 13 and 14). These junctions were characterized by PF faces with intramembrane particles arranged in tetragonal arrays, 6–7 nm in unit cell dimension, and smooth EF faces devoid of particles or pits. The size of the arrays was small in thin junctions but far more extensive in wavy junctions. Fig. 13, *A* and *B*, shows gold particles under the tetragonal arrays of intramembrane particles on the PF faces and under smooth EF faces (Fig. 13, *open triangles*). Gold particles were absent, however, from other fracture faces and from the glass surface. Fig. 14 shows the fracture faces of thin junctions in label-fracture replicas. The PF fracture faces of thin junctions were labeled with gold particles under small patches of tetragonal arrays (*arrows*). The EF faces of thin junctions were smooth and were also labeled with the gold particles. An important feature of these EF faces was the absence of pits arranged tetragonally, suggesting that tetragonal arrays are not formed of coaxially aligned channels. The distribution of gold particles in small clusters under extensive and smooth EF fracture faces is more consistent with MIP molecules organized in a staggered or checkerboard arrangement.

Wavy junctions were identified by the presence of extensive tetragonal arrays of particles on the PF faces and by the large smooth EF faces. Both faces of wavy junctions were labeled with gold particles. The comparison of fracture faces of thin and wavy junctions indicates that the principal difference between these two types of junctions is in the number of MIP molecules forming the patches. In wavy junctions, MIP forms large patches displaying tetragonal symmetry (Fig. 13, *A* and *B*), while, in thin junctions, MIP is arranged in single molecules or in very small patches (Fig. 14). Thus, the pattern of labeling of thin and wavy junctions observed in label-fracture replicas demonstrates conclusively that one membrane of the junction contains particles and that the apposing one is particle free. These observations demonstrate directly that MIP molecules in one membrane must abut a particle-free membrane to form thin and wavy junctions instead of having coaxially aligned gap junction–like channels spanning both apposed membranes and the intervening extracellular gap.

Discussion

The fundamental structural characteristic of gap junctions is the presence of cell–cell channels formed by the coaxial alignment of two apposing hemichannels (59, 60). This structure provides aqueous pathways directly connecting cell cytoplasms without passing through the extracellular space.

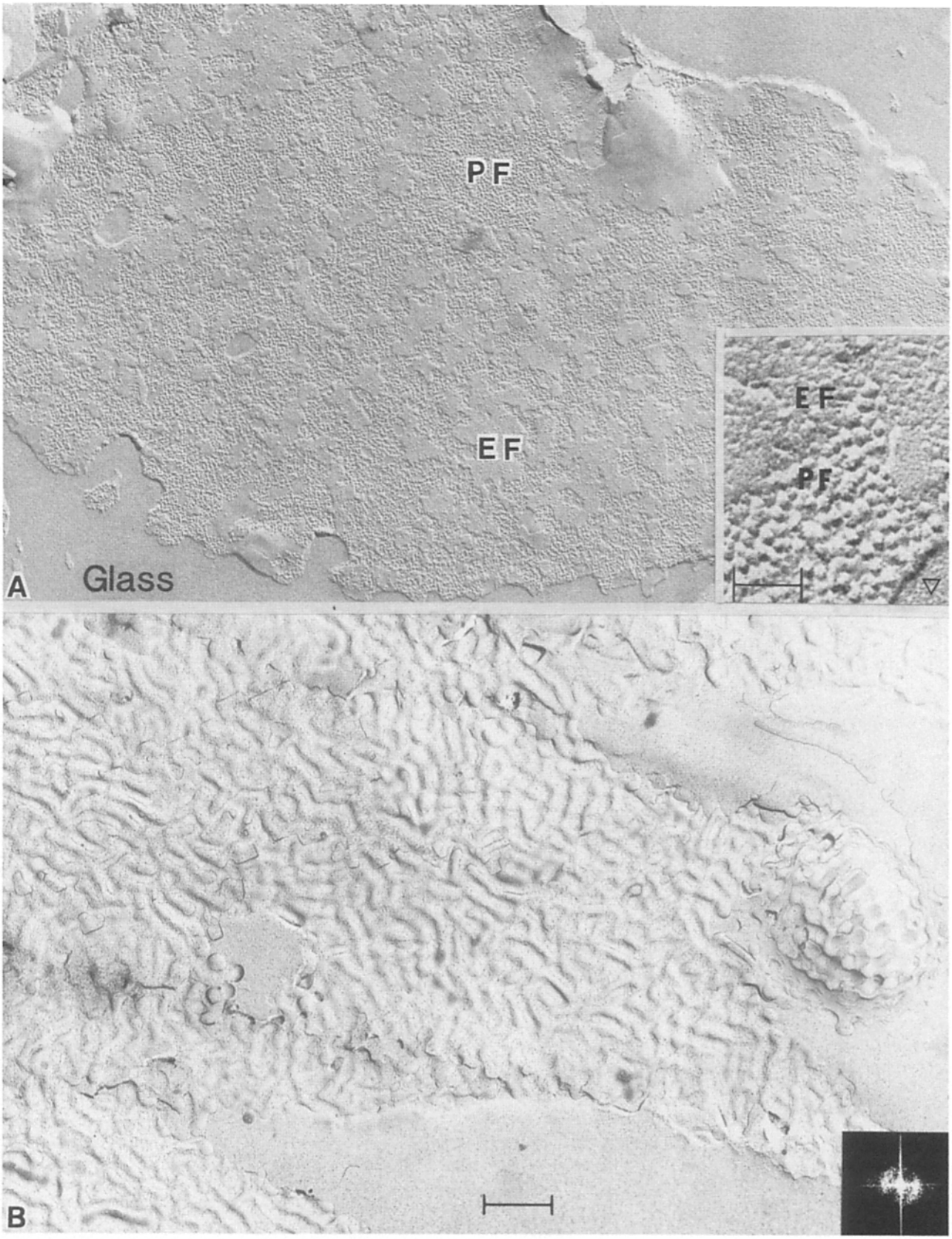

Figure 9. Low magnification view of freeze-fracture replicas of extensive thick (*A*) and wavy (*B*) junctions. The thick junction was fractured after being adhered to a positively charged glass surface. The undulating surface topology of wavy junction (*B*) was observed most clearly in intact bovine lenses. When adhered to glass, wavy junctions lose their undulating topology. The inset in *B* shows an optical transform of a region of the wavy junction; the average period of the wave measured from the position of the first maxima was 0.26 μm. In thick junctions (*A*, *inset*), the fracture plane passed from the glass surface to the hydrophobic cores of the junctional membranes. Junctions can adhere to the glass through the cytoplasmic surfaces only. Thus, PF fracture faces arise exclusively from the membrane attached to the glass. The inset in *A* shows a higher magnification view of the fracture steps separating the PF from the EF faces and the underlying glass substrate (*triangle*). The step separating PF from EF faces corresponds to the distance between the middle of the hydrophobic cores of the junctional membranes (Table I). The steps separating the glass surface from the PF face correspond to one half membrane, while the step separating the glass from the EF face corresponds to one and one half membranes. Bars: (*A* and *B*) 0.75 μm; (*inset*) 75 nm.

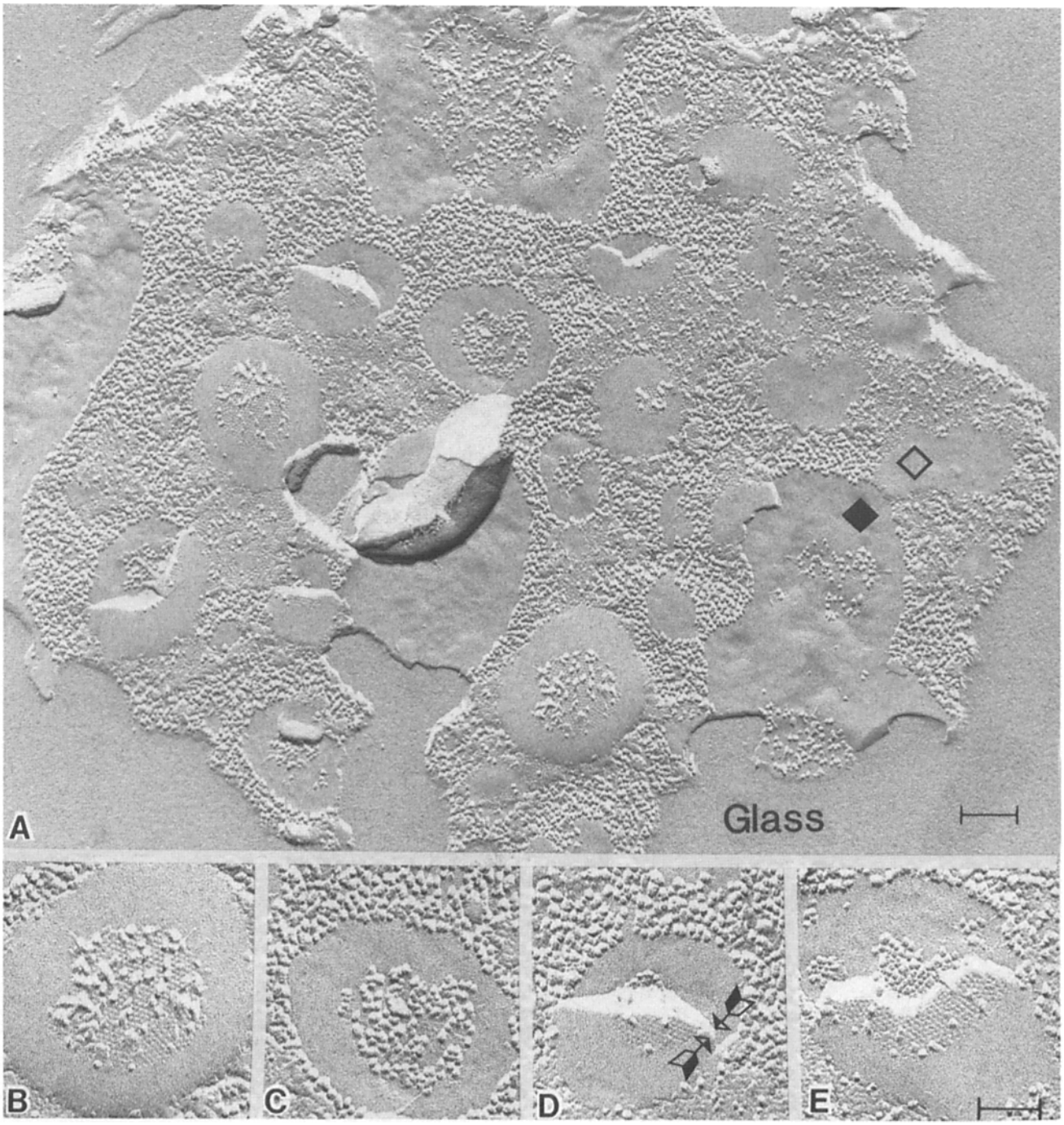

Figure 10. Freeze-fracture replica of a junction displaying fracture patterns with characteristics of both wavy and thick junctions. *A* shows an extensive junction having EF and PF faces with particles and pits arranged randomly and with rounded, dome-like regions (0.2–0.3-μm diameter). There are also plasma membranes with smooth EF (*open square*) and PF (*dark square*) faces. These faces are indicative of regions of protein-free membranes in these junctions. The frequency and size of particle-free membranes appear to increase with lens aging. The domes, on the other hand, contained patches of particles on the PF face and complementary pits on the EF face arranged tetragonally. Usually an annulus of particle-free membrane separated the array from the rest of the junction. The tetragonal arrays of particles and pits located in the domes contrasted sharply with the noncrystalline arrangement of the particles and pits in more flat regions of the junction. When the fracture plane passed across the domes (*D* and *E*), the fracture steps separating EF from PF faces were of large height indicating that the membranes were separated by spaces of large widths (*arrows*, *D*). In *E*, tetragonal arrays are facing each other across a space of large width. Therefore, tetragonal arrays at the domes cannot form coaxially aligned communicating channels. Bars: (*A*) 0.1 μm; (*B–E*) 80 nm.

This study presents evidence that lens wavy junctions consist of tetragonal crystals of MIP in the convex membrane that abut a particle-free concave membrane (Fig. 15). This model of wavy junctions is supported by the direct observation of MIP forming the tetragonal arrays in the convex membrane and by the demonstration that the apposing concave membrane does not contain MIP or any other intrinsic membrane protein. Similar structural organization for wavy junctions

Figure 11. Label-fracture replica of an extensive, predominantly thick junction labeled with the polyclonal anti-MIP and visualized with protein A–gold (15-nm diameter). The plaques were identified as thick junctions because of pits on the EF, particles on the PF faces, fracture steps of small height separating EF and PF faces, and the absence of tetragonal arrays. Junctions with those fracture faces contained only a few gold particles in dome-like regions and as single particles scattered throughout the junctional plane. Note that these gold particles do not cast shadows, therefore, they must be located under the fractured membranes (see Fig. 12). Bars: (*A*) 0.25 μm; (*B*) 80 nm.

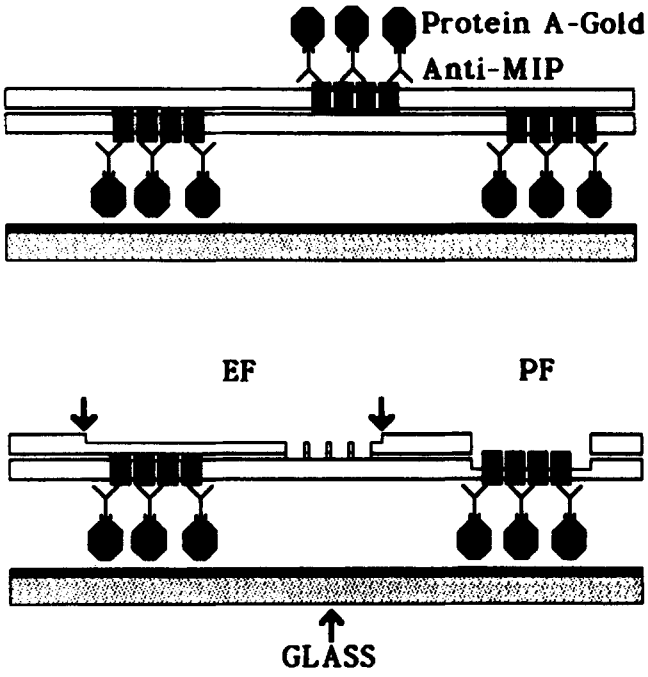

Figure 12. The upper diagram shows a junction constructed of patches of MIP in one membrane abutting a particle-free apposing plasma membrane. The antibody molecules and the gold particles are associated to the cytoplasmic surfaces of the patches of MIP. The lower diagram illustrates the predicted distribution of antibody molecules and gold particles after fracturing. The diagram shows that only the particles labeling the membrane attached to the glass can be observed in the replicas. The model predicts that gold particles under EF faces are covered by one and one half membranes while gold particles under PF faces are covered by one half membrane. If the junctions containing MIP are constructed of coaxial aligned channels, then gold particles must be observed with equal frequency under PF faces and EF faces containing particles and pits arranged tetragonally. The fact that EF faces are smooth indicates that these junctions lack a central plane of symmetry.

had also been derived from freeze-fracture studies of human lenses (36) and in isolated junctions from bovine lenses (9).

The width of the extracellular gap of wavy junctions was calculated by subtracting the physical thickness of a 1:1 lecithin/cholesterol bilayer (5 nm) (35) from the measured distance between the centers of the hydrophobic cores (5.7 nm). A gap of 0.7 nm in width is much smaller than the gap of liver gap junctions (3 nm). Moreover, such a gap could accommodate at most a layer 2–3 water molecules thick or 1–2 amino acids thick. If lens plasma membranes were thinner than a lecithin/cholesterol bilayer by 0.5 nm (a 1:1 lecithin/cholesterol being chosen as a close approximation to the lipid composition of the lens), then the calculated width of the gap would increase to 1.2 nm or the width of approximately four water molecules. Such change would not alter any of the con-

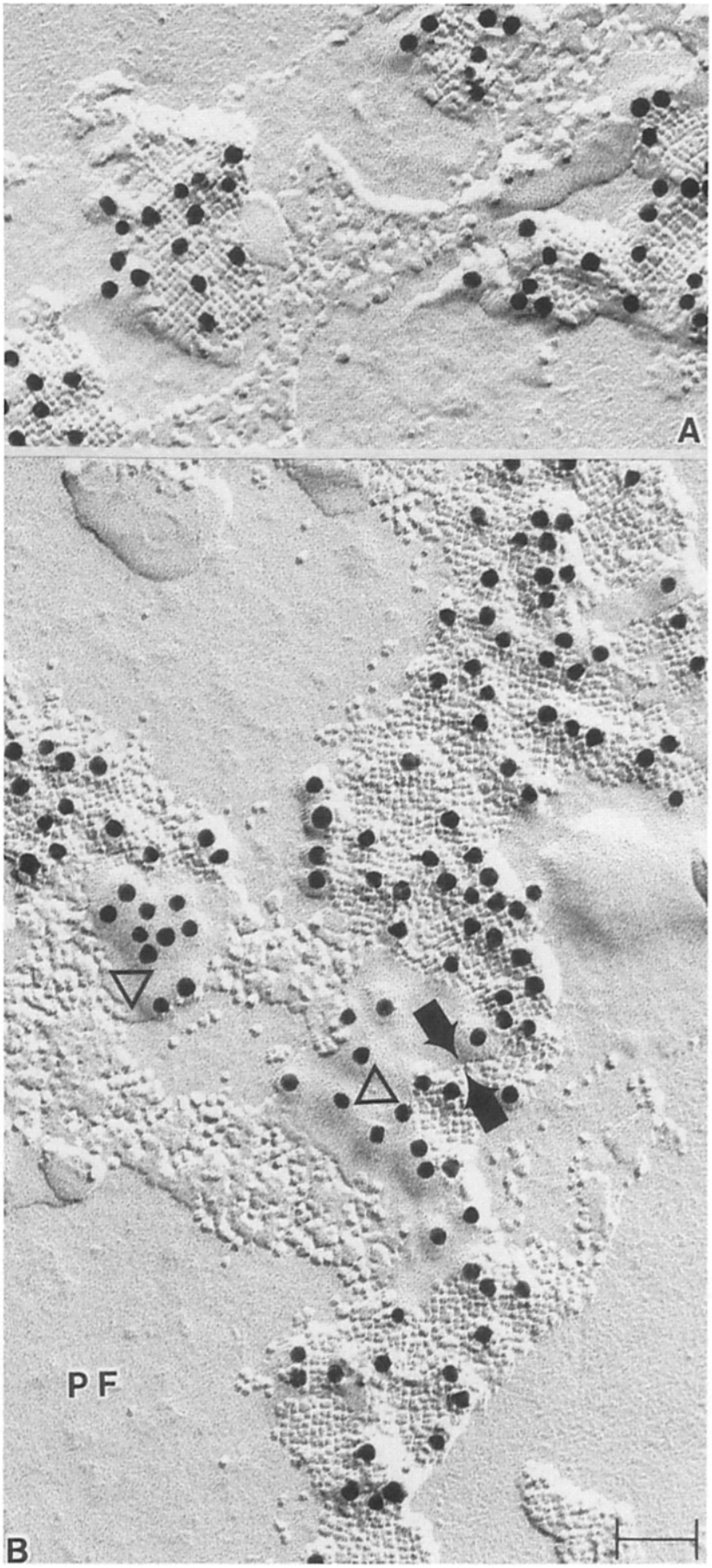

Figure 13. Label-fracture replica of junctions labeled with the polyclonal anti-MIP visualized with gold particles. In *A*, gold particles were associated exclusively with patches of tetragonal arrays of particles on the PF faces. Fracture faces of other membranes without intramembrane particles arranged in crystals remained unlabeled. *B* shows an extensive PF face of a tetragonal crystal labeled with the gold particles. In addition to the tetragonal arrays, gold particles were present under smooth EF faces (*open triangle*). The tetragonal arrays were separated from the smooth EF faces by fracture steps of small height indicating the presence of small intervening gaps (*black arrows*). Therefore, the EF and PF fracture faces labeled with gold particles most likely correspond to wavy junctions. The fact that EF faces do not contain pits arranged tetragonally indicate that tetragonal arrays are apposed to particle-free membranes. Thus, wavy junctions do not contain coaxial aligned channels (see Figs. 12 and 15). Bar, 62.5 nm.

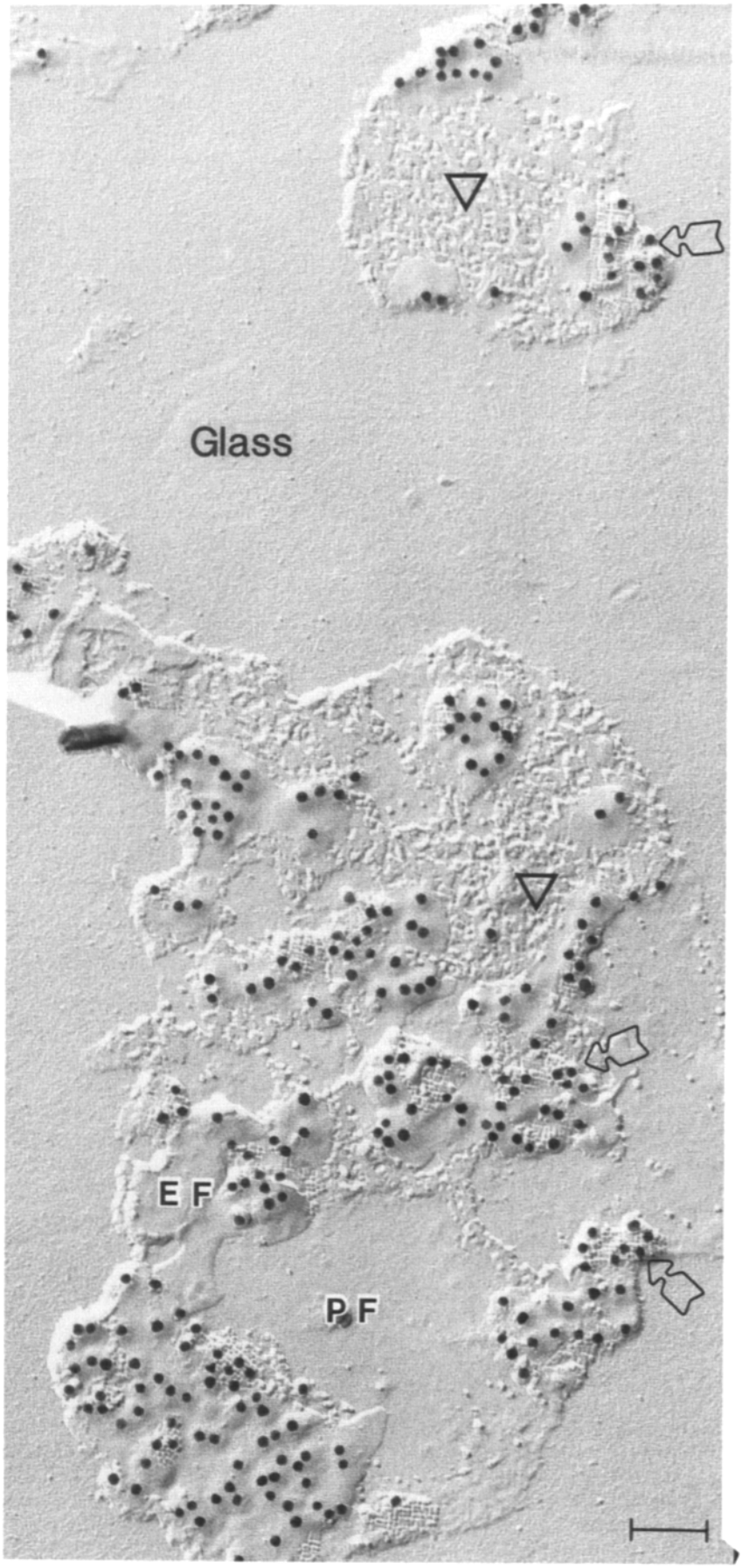

Figure 14. Label-fracture replica of thin junctions labeled with the polyclonal anti-MIP. Gold particles were located under extensive smooth EF faces and under PF faces containing tetragonal arrays of particles. Gold particles were absent from the glass surface, from the particle-free membrane faces (*PF*), and from small regions of thick junctions (*triangles*). The open arrows point to regions where the fracture plane passed from the glass surface to the PF face containing the tetragonal arrays. Note that the gold particles do not cast shadows; therefore, they must be located underneath the fracture membranes. Bar, 0.1 μm.

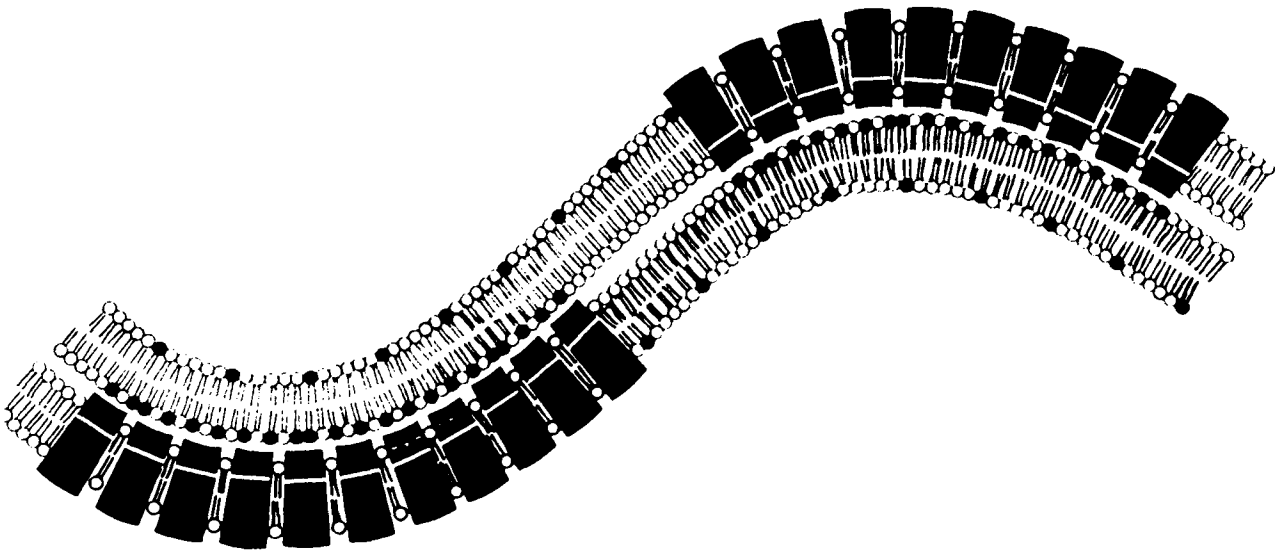

Figure 15. Model explaining the structural organization of MIP in wavy junctions. MIP is arranged in large crystals with tetragonal symmetry in the convex membrane. The crystal abuts an apposing particle-free, concave membrane leaving a small intervening gap. The undulation observed in the junction is produced by a grouping of charged residues or the shape of the molecule that must have a cross-sectional area larger in the cytoplasmic domain than in the external domain. In thin junctions, small clusters and single molecules of MIP also abut a particle-free apposing membrane in a staggered or checkerboard pattern. Therefore, the structural organizations of MIP in thin and wavy junctions differ only in the size of the crystalline patches. Thin junctions lack the curvature of wavy junctions because the patches in opposite membranes have a tendency to bend in opposite directions, thus cancelling the bending movements generated by the intrinsic curvature. The model proposes that the junctions are most likely stabilized by electrostatic attraction between positively charged amino acids located in the external domain of the molecule and negatively charged lipids on the opposing membrane (*blackhead groups*).

clusions presented here. Thus, the structural organization of MIP eliminates the wavy junctions from a function in lens cell communication via gap junctions.

In thin junctions, MIP is organized as individual tetramers or in small patches also abutting an apposing particle-free membrane. The small clusters and single molecules of MIP appear to be arranged in a staggered or checkerboard pattern. Such a model for thin junctions is supported by evidence gathered from label-fracture replicas (Figs. 13 and 14), from transverse thin sections showing antibody staining on both apposing junctional membranes with varying degrees of asymmetry (Fig. 5), and from the small width of the extracellular gap (Table I). In particular, the observation of varying degrees of asymmetry in the antibody staining of thin junctions (Fig. 5, *open arrows*) indicates an unequal distribution of MIP molecules in the apposing membranes of these junctions. The functional role of a junction composed of MIP molecules in one membrane abutting a particle-free apposing membrane is also inconsistent with function in cell communication via gap junctions.

A principal difference between wavy and thin junctions is the characteristic undulating surface topology of wavy junctions having a mean wavelength of 0.26 μm. A possible explanation of the precise radius of curvature of wavy junctions might reside in the intrinsic shape (or in a particular grouping of charged residues) of MIP and in its strong tendency to crystallize in two dimensions. To induce curvature in the cystal, the MIP tetramer should have a conical shape with the smaller cross-sectional area toward the external surface of the membrane (25). In contrast with the undulating topology of wavy junctions, thin junctions are flat. A possible explanation of this difference in surface topologies between thin and wavy junctions could be found in the observation that, in thin junctions, MIP is aggregated in small patches and/or single molecules. The small patches in the apposing membranes would have a tendency to bend in opposite directions, thus cancelling the bending moments generated by the intrinsic curvature of the protein. Of course, if thin junctions are constructed of noncrystalline molecules of MIP, there is no bending moment generated, and one would expect the membranes to be flat.

An important conclusion of this study is that both thin and wavy junctions have the same basic structural organization (i.e., MIP tetramers abut a particle-free membrane). Thin and wavy junctions differ only in the extent of crystallization of MIP, a process that depends on lens fiber age. Since MIP is more resistant to endogeneous proteolysis than any other intrinsic membrane proteins of the fiber plasma membrane, wavy junctions are probably formed spontaneously from thin junctions during lens aging by the relative increase in the concentration of MIP that would promote crystallization into larger tetragonal patches. It is this strong tendency of MIP to crystallize in two dimensions which, if taken into account, can explain the different antibody staining patterns observed in this study and also published previously (5, 13, 46, 54). When MIP patches are small, or the molecules exist as monomers, the junctions are flat and the staining pattern is symmetric (Fig. 5, *open arrows*). When MIP forms large crystals, the junctions are wavy and the antibody staining is asymmetric (Fig. 4). Thus, MIP displays two different antibody labeling patterns depending on the extent of crystallization which in turn depends on the age of the fiber cell.

As suggested by Costello et al. (9a), the ability of MIP to produce extraordinarily close membrane-membrane apposi-

tion is consistent with topological models deduced from sequence data (20, 53). In these models, the extracellular domain contains 3–5 positively charged amino acids and no carboxylic amino acids per polypeptide (12–20 per tetramer) or equivalently one charge per 1.2–2.1 nm^2 of crystal surface. Such a charge density would cause tetramers from apposing membranes to repel each other but to attract negatively charged phospholipids in the apposing membrane. Such electrostatic attraction would produce junctions having extremely narrow extracellular spaces. The predictions derived from the sequence data are supported by the observation that in dome-like regions, crystals of MIP in apposing membranes are separated by wide spaces (Fig. 10, *D* and *E*). Thus, it is possible that electrostatic repulsion destabilizes the formation of coaxially aligned channels made of MIP but promotes the interaction between MIP and the apposing particle-free membranes.

A detailed understanding of the significance of MIP in lens physiology should take into account the channel-forming potential of this protein. This property has been established by reconstituting the purified protein into both unilamellar liposomes (15, 44) and planar lipid bilayers (10, 16, 17, 22, 65). These studies have shown that nonelectrolytes as large as maltoheptose (1,152 D) (44) can permeate liposomes containing MIP. In planar lipid bilayers, MIP forms discrete voltage-dependent channels that have an open conductance of ~360 pS and that are poorly selective (10, 22, 65). MIP channels have single channel properties similar to those of gap junction channels between pairs of myocytes (61), lacrimal cells (41), embryonic muscle (8), and pancreatic acinar cells (57) recorded in whole-cell patch clamps. Moreover, MIP's single-channel properties are qualitatively very similar to those exhibited by the channels produced by the reconstitution of the purified rat liver gap junction protein in planar bilayers (62). In spite of the similarities of the properties of MIP channels and gap junction channels recorded between cell pairs, reconstitution studies do not prove that MIP channels are the lens gap junction channels because their coaxial alignment in double membranes has not been demonstrated.

Any proposals for the role of MIP in lens physiology are constricted by certain experimental observations: MIP is found in both single and junctional membranes, MIP cannot form communicating "gap" junction channels in thin and wavy junctions, and MIP does form channels in vesicles and planar bilayers. A possible role of MIP consistent with these constraints might be to minimize extracellular space between lens fibers (64). The mechanism would be as follows. In closely apposed junctional membranes, there would be little transport of ions and water through MIP channels. This would follow from the large resistance of the extracellular space which would restrict flow. In junctional membranes, MIP would function principally to promote cell adhesion. On the other hand, if the junctions were to separate and an isolated pocket of fluid to form between fibers, a channel with the properties of an MIP channel seen in bilayers would promote an influx of solutes followed by water from the extracellular space into the protein-rich fiber cytoplasm in an attempt to reach Donnan equilibrium. The extracellular fluid space would decrease and the apposing membranes would come together to reform the junctions. The channel properties of MIP in bilayers suggest an additional mechanism that could protect the lens fiber cells. If the pockets were isolated in the interior of the lens, its electrical potential would be close to that of the fiber cell because the conductance of a single MIP channel is large compared to that of the extracellular resistance. On the other hand, if the pocket is connected by a low resistance pathway to the bulk extracellular fluid, the voltage across the channel would cause it to close. This could prevent disastrous overload of the lens transport mechanisms. It is the paucity of extracellular space bounded by membranes having channels of potentially high conductance that has not been considered when interpreting electrical measurements suggesting that the lens behaves as a syncytium.

As previously reported (21, 29), MP70 is present in both junctional membranes of thick junctions but absent from thin and wavy junction and single membranes. When compared to liver gap junctions, thick junctions display a larger overall thickness (18–20 nm) and an extracellular gap of smaller width (2 nm). Also, the dense layers at the cytoplasmic surfaces are thicker than those of liver gap junctions and the "in plane" organization of the protein units lacks the characteristic hexagonal symmetry of gap junctions. Label-fracture and double labeling experiments demonstrated the presence of clusters of MIP in thick junctions (Fig. 11). In fact, most junctional profiles isolated from calf lenses contained mixtures of these two proteins at various mole ratios. In these junctions, MIP always tended to phase separately probably as a result of the strong tendency of this protein to form two-dimensional crystals and adhere to the apposing membranes. Upon lens aging, the concentration of MP70 decreases because of endogenous proteolysis, while the relative concentration of MIP (more resistant to proteolysis) increases, resulting in MIP crystallization and wavy junction formation. Thus, the changes in surface topology and protein composition occurring in lens plasma membranes can be explained as a normal aging process.

Unlike the structure of MIP-containing junctions, that of MP70-containing junctions cannot be deduced from the data presented in this paper or available in the literature. It remains a distinct possibility that thick junctions contain gap junction channels spanning both plasma membranes and the intervening extracellular gap, perhaps formed from MP70. However, it must be emphasized that symmetry in antibody staining cannot be equated with the presence of coaxially aligned gap junction–type channels. As for thin junctions containing MIP, small patches or single molecules arranged in a staggered configuration can also produce symmetric antibody staining. Thus, large-scale isolation, reconstitution, and structural analysis in three dimensions would be required to demonstrate that MP70 forms coaxially aligned channels that can function in lens cell communication.

We are thankful for the excellent technical assistance of Mr. M. Kreman and the drawings of Miss P. Zampighi.

This work was supported by National Institutes of Health grants EY04110, EY05661, and NS20669. The support of the Jerry Lewis Neuromuscular Research Center is also acknowledged.

Received for publication 16 August 1988 and in revised form 8 February 1989.

References

1. Alcala, J., N. Lieska, and H. Maisel. 1975. Protein component of bovine lens cortical fiber cell membranes. *Exp. Eye Res.* 21:581–595.
2. Benedetti, E. L., I. Dunia, C. J. Bentzel, A. J. M. Vermorken, M. Kibbelaar, and H. Bloemendal. 1976. A portrait of plasma membrane spe-

cializations in eye lens epithelium and fibers. *Biochim. Biophys. Acta.* 457:353–384.
3. Bernardini, G., and C. Peracchia. 1981. Gap junction crystallization in lens fiber after an increase in cell calcium. *Invest. Ophthalmol. & Visual Sci.* 21:291–299.
4. Beyer, E., D. Paul, and D. A. Goodenough. 1987. Connexin43: a protein from rat heart homologous to a gap junction protein from liver. *J. Cell Biol.* 105:2621–2629.
5. Bok, D., J. Dockstader, and J. Horwitz. 1982. Immunocytochemical localization of the lens main intrinsic protein (MIP26) in communicating junctions. *J. Cell Biol.* 92:213–220.
6. Broekhuyse, R. M., and E. D. Kuhlmann. 1978. Lens membranes IV: preparative isolation and characterization of membranes and various membrane proteins from calf lenses. *Exp. Eye Res.* 26:305–320.
7. Broekhuyse, R. M., E. D. Kuhlmann, and H. J. Winkins. 1979. Lens membranes VII: MIP is an immunologically specific component of lens fiber membranes and is identical with 26K band protein. *Exp. Eye Res.* 29: 303–313.
8. Chow, I., and S. H. Young. 1987. Opening of single gap junction channels during formation of electrical coupling between embryonic muscle cells. *Dev. Biol.* 122:332–337.
9. Costello, M. J., T. J. McIntosh, and J. D. Robertson. 1985. Membrane specializations in mammalian lens fiber cells: distribution of square arrays. *Curr. Eye Res.* 4:1183–1201.
9a. Costello, M. J., T. J. McIntosh, and J. D. Robertson. 1989. Distribution of gap junctions and square array junctions in the mammalian lens. *Invest. Ophthalmol. & Visual Sci.* In press.
10. Ehring, G. R., G. Zampighi, and J. E. Hall. 1988. Properties of MIP channels reconsituted in planar lipid bilayers. *In* Gap Junctions. E. L. Hertzberg and R. Johnson, editors. Alan R. Liss, Inc., New York. 335–346.
11. Fisher, K. A. 1975. "Half" membrane enrichment: verification by electron microscopy. *Science (Wash. DC).* 190:983–985.
12. Deleted in proof.
13. Fitzgerald, P. G., D. Bok, and J. Horwitz. 1983. Immunocytochemical localization of the main intrinsic polypeptide (MIP) in ultrathin frozen sections of rat lens. *J. Cell Biol.* 97:1491–1499.
14. Gimlich, R. L., N. M. Kumar, and N. B. Gilula. 1988. Sequence and developmental expression of mRNA coding for a gap junction protein in *Xenopus*. *J. Cell Biol.* 107:1065–1073.
15. Girsch, S. J., and C. Peracchia. 1985. Lens cell-to-cell channel protein. I. Self-assembly into liposomes and permeability regulation by calmodulin. *J. Membr. Biol.* 83:217–225.
16. Gooden, M. M., L. J. Takemoto, and D. A. Rintoul. 1985. Reconstitution of MIP26 from single human lenses into artificial membranes. I. Differences in pH sensitivity of cataractous vs. normal human lens fiber cell proteins. *Curr. Eye Res.* 4:1107–1115.
17. Gooden, M. M., D. A. Rintoul, M. Takehana, and L. J. Takemoto. 1985. Major intrinsic polypeptide (MIP26) from lens membrane: reconstitution into vesicles and inhibition of channel forming activity by peptide antiserum. *Biochem. Biophys. Res. Commun.* 128:993–999.
18. Goodenough, D. A. 1979. Lens gap junctions: a structural hypothesis for non-regulated low resistance intercellular pathways. *Invest. Ophthalmol. & Visual Sci.* 18:1104–1122.
19. Goodenough, D. A., J. S. B. Dick II, and J. E. Lyons. 1980. Lens metabolic cooperation: a study of mouse lens transport and permeability visualized with freeze-substitution autoradiography and electron microscopy. *J. Cell Biol.* 86:576–589.
20. Gorin, M. B., S. B. Yancey, J. Cline, J. P. Revel, and J. Horwitz. 1984. The major intrinsic protein (MIP) of the bovine fiber membrane: characterization and structure based on cDNA cloning. *Cell.* 39:49–59.
21. Gruijters, W. T. M., J. Kistler, S. Bullivant, and D. A. Goodenough. 1987. Immunolocalization of MP70 in lens fiber 16–17-nm intercellular junctions. *J. Cell Biol.* 104:565–572.
22. Hall, J. E., and G. A. Zampighi. 1985. Protein from purfied lens junctions induces channels in planar lipid bilayers. *In* Gap Junctions. M. V. L. Bennett and D. C. Spray, editors. Cold Spring Harbor Laboratory, Cold Spring Harbor, NY. 117–189.
23. Hertzberg, E. L., D. J. Anderson, M. Friedlander, and N. B. Gilula. 1982. Comparative analysis of the major polypeptides from liver gap junctions and lens fiber junctions. *J. Cell Biol.* 92:53–59.
24. Horwitz, J., and M. M. Wong. 1980. Peptide mapping by limited proteolysis in sodium dodecylsulphate of the main intrinsic polypeptides isolated from human and bovine lens plasma membranes. *Biochim. Biophys. Acta.* 622:134–143.
25. Israelachbili, J. N. 1985. Intermolecular and Surface Forces. Academic Press Inc., New York. 161–193; 246–264.
26. Keeling, P., K. Johnson, D. Sas, P. Donahue, and R. Jonhson. 1983. Arrangement of MIP 26 in lens junctional membranes: analysis with protease and antibodies. *J. Membr. Biol.* 74:217–228.
27. Deleted in proof.
28. Kistler, J., and S. Bullivant. 1987. Proteins in lens intracellular junctions: cleavage of MP70 to MP38. *Invest. Ophthalmol. & Visual Sci.* 28: 1687–1692.
29. Kistler, J., B. Kirkland, and S. Bullivant. 1985. Identification of a 70,000-D protein in lens membrane junctional domains. *J. Cell Biol.* 101:28–35.
30. Kistler, J., D. Christie, and S. Bullivant. 1988. Homologies between gap junction proteins in lens, heart, and liver. *Nature (Lond.).* 331:721–723.
31. Kumar, N., and N. B. Gilula. 1986. Cloning and characterization of human and rat liver cDNAs coding for a gap junction protein. *J. Cell Biol.* 103:767–776.
32. Kuszak, J. R., J. L. Rae, B. U. Pauli, and R. S. Weinstein. 1982. Rotary replication of lens gap junctions. *J. Ultrastruct. Res.* 81:249–256.
33. Kuszak, J. R., Y. H. Shek, K. C. Carney, and J. L. Rae. 1985. A correlative freeze-etch and electrophysiological study of communicating junctions in crystalline lenses. *Curr. Eye Res.* 4:1145–1153.
34. Kuwabara, T. 1975. The maturation of the lens cell: a morphological study. *Exp. Eye Res.* 20:427–443.
35. Lecuyer, H., and D. G. Dervichian. 1969. Structure of aqueous mixtures of lecithin and cholesterol. *J. Mol. Biol.* 45:39–57.
36. Lo, W. K., and C. V. Harding. 1984. Square arrays and their role in ridge formation in human lens fibers. *J. Ultrastruct. Res.* 86:228–245.
37. Lowry, O. H., N. J. Rosebrough, A. L. Farr, and R. J. Randall. 1951. Protein measurement with the Folin phenol reagent. *J. Biol. Chem.* 193: 265–275.
38. Mathias, R. T., and J. L. Rae. 1985. Transport properties of the lens. *Am. J. Physiol.* 249:C181–C190.
39. Mathias, R. T., J. L. Rae, and R. S. Eisenberg. 1982. The lens as a nonuniform spherical syncytium. *Biophys. J.* 34:61–83.
40. Miller, T. M., and D. A. Goodenough. 1985. Gap junction structures after experimental alteration of junctional channel conductance. *J. Cell Biol.* 101:1741–1748.
41. Neyton, J., and A. Trautmann. 1985. Single-channel currents of an intercellular junction. *Nature (Lond.).* 317:331–335.
42. Ngoc, L. D., P. Paroutaud, I. Dunia, E. L. Benedetti, and J. Hoebeke. 1985. Sequence analysis of peptide fragments from the intrinsic membrane protein of calf lens fibers MP26 and its natural maturation product MP22. *FEBS (Fed. Eur. Biochem. Soc.) Lett.* 181:74–78.
43. Nicholson, B. J., L. J. Takemoto, M. W. Hunkapiller, L. E. Hood, and J. P. Revel. 1983. Differences between liver gap junction protein and lens MIP 26 from rat: implications for tissue specificity of gap junctions. *Cell.* 32:967–978.
44. Nikaido, H., and E. Y. Rosenberg. 1985. Functional reconstitution of lens gap junction proteins into proteoliposomes. *J. Membr. Biol.* 85:87–92.
45. Okinami, S. 1978. Freeze-fracture replicas of the primate lens fibers. *Albrecht von Graefes Arch. Klin. Exp. Ophthalmol.* 209:51–58.
46. Paul, D. 1986. Molecular cloning of cDNA for rat liver gap junction protein. *J. Cell Biol.* 103:123–134.
47. Paul, D., and D. A. Goodenough. 1983. Preparation, localization and characterization of antisera against bovine MP26, an integral protein from lens fiber plasma membrane. *J. Cell Biol.* 96:625–632.
48. Peracchia, C., and L. L. Peracchia. 1980. Gap junction dynamics: reversible effects of divalent cations. *J. Cell Biol.* 87:708–718.
49. Peracchia, C., and L. L. Peracchia. 1980. Gap junction dynamics: reversible effects of hydrogen ions. *J. Cell Biol.* 87:273–279.
50. Pinto da Silva, P., and W. K. Khan. 1984. Label-fracture: a method for high resolution labeling of cell surfaces. *J. Cell Biol.* 99:1156–1161.
51. Rae, J. L., and R. A. Lewis. 1984. Patch clamp recordings from the epithelium of the lens obtained using glasses selected for low noise and improved sealing properties. *Biophys. J.* 45:144–146.
52. Rae, J. L., R. D. Thomson, and R. S. Eisenberg. 1982. The effect of 2-4 dinitrophenol on cell to cell communication in the frog lens. *Exp. Eye Res.* 35:597–609.
53. Revel, J. P., and S. B. Yancey. 1985. Molecular conformation of the major intrinsic protein of the lens fiber membrane: is it a junction protein? *In* Gap Junctions. M. V. L. Bennett and D. C. Spray, editors. Cold Spring Harbor Laboratory, Gold Spring Harbor, NY. 33–48.
54. Sas, D. F., M. J. Sas, K. R. Johnson, A. S. Menko, and R. G. Johnson. 1985. Junctions between lens fibers are labeled with a monoclonal antibody shown to be specific for MP26. *J. Cell Biol.* 100:216–275.
55. Schuetzy, S. M., and D. A. Goodenough. 1982. Dye transfer between cells of the embryonic chick becomes lens sensitive to CO2 treatment with development. *J. Cell Biol.* 92:694–705.
56. Simon, S. A., G. Zampighi, T. J. McIntosh. M. J. Costello, H. P. Ting-Beall, and J. D. Robertson. 1982. The structure of junctions between lens fiber cells. *Biosci. Rep.* 2:333–341.
57. Somogyi, R., and A. Kolb. 1988. Cell-to-cell channel conductance during loss of gap junction coupling in pairs of pancreatic acinar and Chinese hamster ovary cells. *Pfluegers Arch. Eur. J. Physiol.* 412:54–65.
58. Takemoto, L. J., J. S. Hansen, and J. Horwitz. 1981. Interspecies conservation of the main intrinsic polypeptide (MIP) of the lens membrane. *Comp. Biochem. Physiol. B. Comp. Biochem.* 68:101–106.
59. Unwin, P. N. T., and P. D. Ennis. 1984. Two configurations of a channel forming membrane protein. *Nature (Lond.).* 307:609–613.
60. Unwin, P. N. T., and G. Zampighi. 1980. Structure of junctions between communicating cells. *Nature (Lond.).* 283:545–549.
61. Veenstra, R. D., and R. L. DeHaan. 1986. Measurement of single channel currents from cardiac gap junctions. *Science (Wash. DC).* 233:972–974.
62. Young, J. D. E., Z. A. Cohn, and N. B. Gilula. 1987. Functional assembly of gap junction conductance in lipid bilayers: demonstration that the major 27 kd protein forms the junctional channel. *Cell.* 48:733–743.

63. Deleted in proof.
64. Zampighi, G., S. A. Simon, J. D. Robertson, T. J. McIntosh, and M. J. Costello. 1982. On the structural organization of isolated bovine lens fiber junctions. *J. Cell Biol.* 93:175–189.
65. Zampighi, G., J. E. Hall, and M. Kreman. 1985. Purified lens junctional protein forms channels in planar lipid films. *Proc. Natl. Acad. Sci. USA.* 82:8468–8472.
66. Zampighi, G., M. Kreman, F. Ramon, A. L. Moreno, and S. A. Simon. 1988. Structural characteristics of gap junctions. I. Channel number in coupled and uncoupled conditions. *J. Cell Biol.* 106:1667–1678.